Technical Note: Modeling the mineral dust aerosol cycle in ALADIN

Simulation of the March 7-13 West Africa dust storm

Mohamed Mokhtari[1]

[1] *Office National de la Météorologie (ONM- Algérie)*

Substantial impacts of dust aerosol on climate and environment have increased, that why there is a need to better understand and eventually predict the atmospheric dust cycle. Along these lines, several dust models have been developed *[Tegen and Fung, 1994; Nickovic and Dobricic, 1996; Nickovic et al., 2001]* and used for studying dust processes. The major phases of the atmospheric dust cycle consists on : emission, transport, wet and dry deposition. In this work, the atmospheric dust cycle has been integrated in ALADIN model. The emission processes are treated in SURFEX (SURFace EXternalisée) by the DEAD module (Dust Entrainment And Deposition) *[Grini and al., 2006]*. The first step consists of an improvement of the dust emission scheme (version SURFEX) by introducing the soil aggregate distribution and size-depending energy thresholds for particle release during sandblasting *[Alfaro and Gomes, 2001]*. The second step deals with the treatment of the transport and the removal processes of dust aerosols in ALADIN. The coupled ALADIN_SURFEX system is used to simulate the March 7-13 West Africa dust storm. To validate the results, we used the daily mean AOD (Aerosol Optical Depth) from AQUA-MODIS satellite data and the local AOD and concentration measurements available in the African Monsoon Multidisciplinary Analyses (AMMA) data base.

1. Introduction

Mineral dust aerosol has an important impact on the climate and the environment. It is involved in the direct radiative forcing processes *[Tegen et al., 1996]*, nutrient transport *[Martin, 1990; Swap et al., 1992]*, Land-use change *[Nicholson et al., 2000]* and ecosystem heath *[Prospero, 1999; Shinn et al., 2000]*. Therefore, it is important to include the description of dust aerosols processes in the atmospheric models. The first difficulty to evaluate the impact of the dust aerosols on climate and environment is to determine correctly their concentration in the atmosphere. To achieve this, it is necessary to be able to represent rigorously the quantities which are injected in the atmosphere and also we have to evaluate their intensity, extension and frequency.

The mineral dust emissions from the arid and semi-arid areas are strongly influenced by the surface characteristics. The surface features controls three major processes of dust production: the erosion threshold wind velocity, the wind shear-stress which acts on the erodible surface and the capability of the soil to release fine dust particles. Recently, many models of dust emission have been developed in order to provide an explicit representation of the mineral dust emission processes and the influence of the surface features. These models are often differentiated by their representation of mobilization. According to *Zender et al. [2003],* two categories of model are distinguished. The simpler class, named the bulk mobilization schemes, parameterize mobilization in terms of the third

or fourth power of the wind speed or wind friction speed include those of *Tegen and Fung [1994], Mahowald and al. [1999],* and *Perlwitz and al. [2001]*. The more complex class use complete microphysical specification of the erodible environment to predict the size-resolved saltation mass flux and resulting sandblasted dust emissions *[Marticorena and Bergametti, 1995; Shao and al, 1996; Shao, 2001]*. At regional simulation, these schemes have shown promising results *[Shao and leslie, 1997; Marticorena and Al, 1997]*. But, globally many of the input for these fully microphysical are not known.

DEAD is an intermediate scheme in term of complexity, between these two extremes. It is developed by *Zender et al. [2003]* and used in global simulations. This scheme is coupled with SURFEX *[Grini and al 2006]*. In SURFEX version, this scheme assumes that the soil textures is globally uniform and is replete with particles diameter of 75 µm *[Zender et al., 2003]*. The saltation flux calculated for this type of particle is weighted with the fraction of Sand available in the soil *[Grini et al., 2006]*. The transfer function between the horizontal saltation flux and the vertical mass flux (α) is calculated by *Marticorena and Bergametti* relationships *[1995]*. DEAD assume that a globally uniform value of $M_{clay} = 0.2$ is the right value to determine the sandblasting mass efficiency α *[Zender et al., 2003]*.

DEAD omits some important processes being able to influence the dust emission: geographic variation of surface size distribution *[Marticorena et al., 1997]*, size-dependent energy thresholds for particle release during sandblasting *[Alfaro et Gomes, 2001]*. These limits could be performed in SURFEX scheme using ECOCLIMAP database providing information on the erodible fraction (represented by the COVER004 and COVER005 relating to the bare and rock soil) *[Masson et al., 2003]* and FAO databases containing information on the sand, silt and clay fraction allowing a classification of the soil textures.

In this work, we integrate the atmospheric aerosol dust cycle in ALADIN model. For the surface processes we propose to improve the mineral dust emission scheme by adding the soil aggregate distribution and to choose the most compatible parameterization with SURFEX databases. The advection, diffusion and removal processes are treated in ALADIN. To evaluate the performance of the coupled system ALADIN_SURFEX in the dust aerosol forecast, we simulate the March 7-13 west Africa dust storm. The results are compared with the daily mean AOD from MODIS/AQUA satellite and the local AOD and mass concentration measurements available in the AMMA database. This notice is organised as follows: section 2 describe the physical model. Section 3 describes the meteorological situation and we present the results. Section 4 presents our summary and concluding remarks.

2. Dust parameterization in ALADIN

2.1 The ALADIN model

ALADIN (Aire Limitée Adaptation Dynamique développement Initialisation) is a spectral hydrostatic model. It is developed in an international cooperation led by Météo France; it is operationally used for weather prediction. ALADIN is a fully three-dimensional baroclinic system of primitive equations using a two-time-level semi-Lagrangian semi-implicit numerical integration scheme and a digital filter initialisation. The main purpose of ALADIN is to perform a dynamical adaptation of forecasts of the global NWP (Numerical Weather Prediction) model ARPEGE to a high resolution *[Huth et al., 2003]*. For its complete scientific description, readers may refer to *Bubnová et al. [1995]*, *Radnóti [1995], Horányi et al. [1996], Geleyn [1998]* and *Váňa [1998]*. The physical parameterization package comprises: gravity wave drag parameterization, Semi-Lagrangian horizontal diffusion (SLDH) computed in spectral space, vertical diffusion and planetary boundary layer parameterisation, Sub-grid scale deep convection and convective precipitations, The RRTM radiation scheme (Rapid Radiative Transfer Model) in long wave *[Mlawer et al., 1997]* and *Fouquart Morcrette* with 6 spectral bands in shortwave, Grid-scale (resolved) clouds and large-scale (stratiform) precipitations developed by *Philippe Lopez [2002],* And externalized surface scheme (SURFEX) for the surface processes: Interaction Soil Biosphere Atmosphere (*ISBA)* scheme *[Noilhan et Planton 1989]*, sea (Ecume fluxes), Town Energy Balance (TEB) [*Masson 2000]* and lakes.

2.2 Modelling mineral dust emissions in SURFEX

The representation of dust emission processes is a key element in a dust model and depends on the wind conditions, soil characteristics and particle size. Here, the dust emission calculation is based on the parameterizations of soil aggregate saltation and sandblasting processes. The main steps in this calculation are: the specification of soil aggregate size distribution for each model grid cell, the calculation of a threshold friction velocity leading to erosion and saltation processes, the calculation of the horizontal saltating soil aggregate mass flux, and finally the calculation of the vertical transportable dust particle mass flux generated by the saltating aggregates.

2.2.1 Emitting area

The dust emitting areas are recognized in SURFEX by the cover COVER004 and COVER005 relative to bare soil and bare rock soil *[Masson et al., 2003]*. These two covers are represented in the figure 1 and 2.

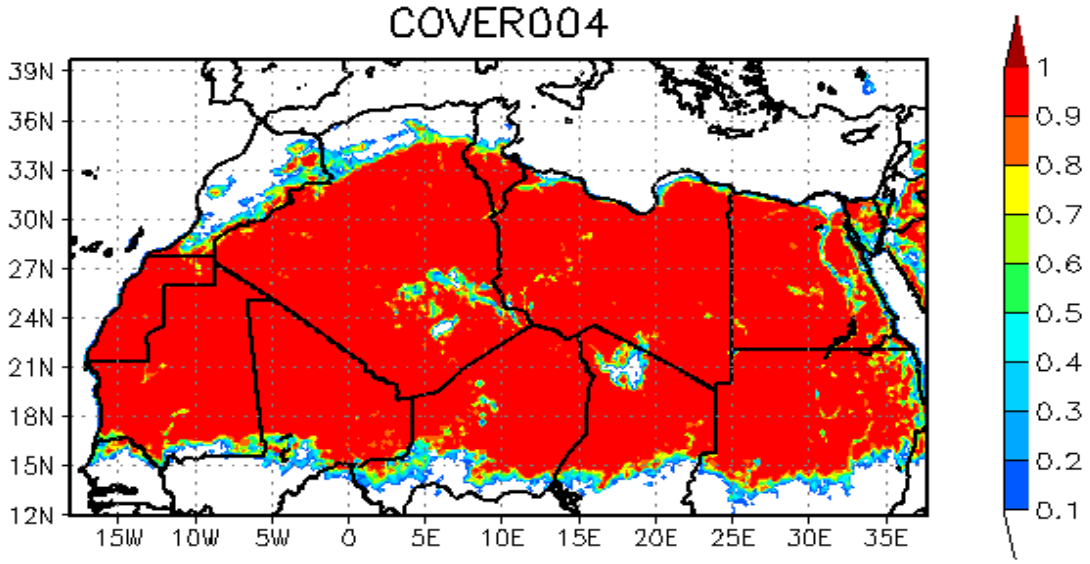

Figure1: COVER004 relatives to bare soil

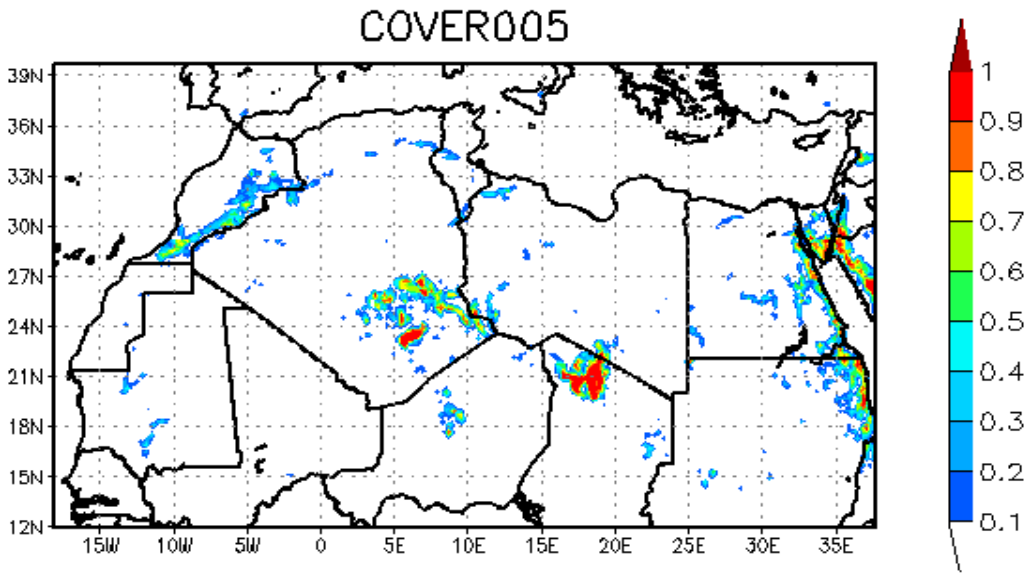

Figure 2: COVER005 relatives to bare rock soil

2.2.2 Soil texture

The knowledge of the soil texture is necessary to determine the potential fine particles in the soil and to control the soil water contents. In order to characterize the erodible fraction of different types of soils, soil aggregate distributions are provided to the model. Basically, these distributions

rely upon the USDA (United States Department of Agriculture) textural classification (Table 1), for which different types of soil are classified according to an index referring to the classic sand/clay/silt triangle of texture composition *[Buckley, 2001]* figure 3.

Table 1 : Soil textures classification following USDA (1998)

	Soil texture		*Soil texture*		*Soil texture*
1	*Sand*	*5*	*Loam*	*9*	*Sandy clay*
2	*Loamy sand*	*6*	*Sandy clay loam*	*10*	*Silty clay*
3	*Sandy loam*	*7*	*Silty clay loam*	*11*	*Clay*
4	*Silt loam*	*8*	*Clay loam*	*12*	*Silt*

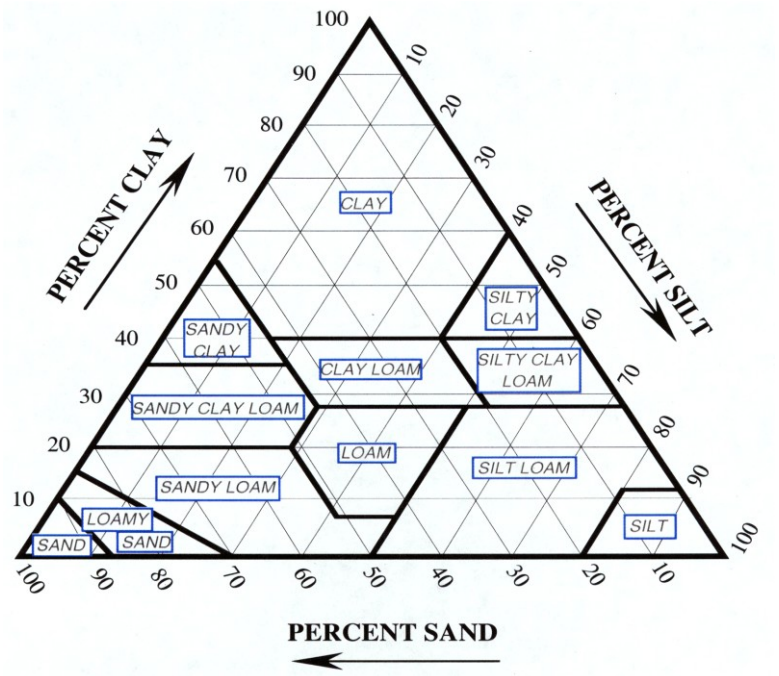

Figure 3 : sand/clay/silt triangle of texture composition according USDA (1998) [Buckley, 2001]

Figures 4, 5 and 6 illustrate the sand/clay/silt fractions from the FAO database used in SURFEX *[Noilhan et al., 1996],* with 10 km horizontal resolution

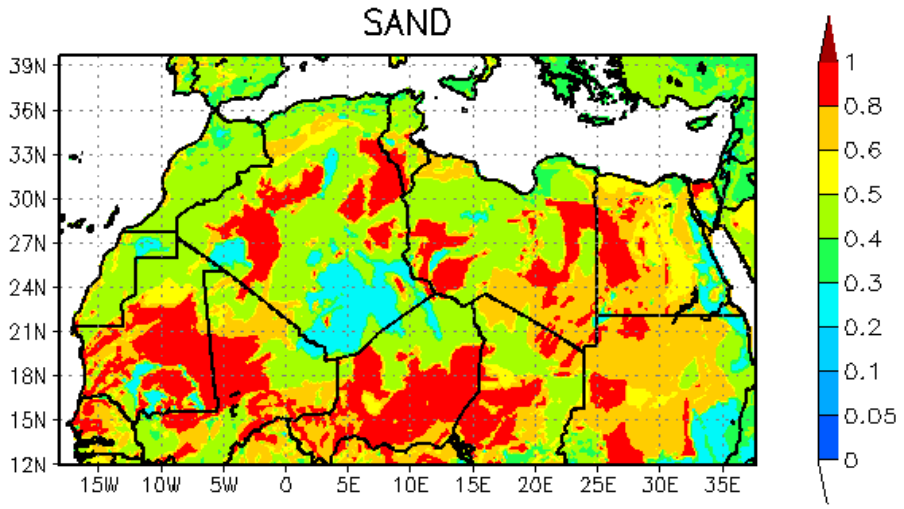

Figure 4: Sand fraction for North Africa

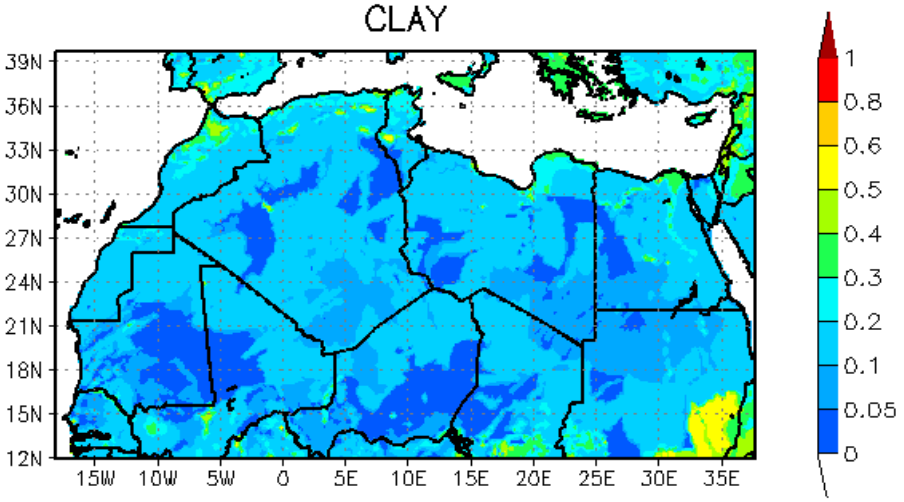

Figure 5: Clay/silt fraction for North Africa

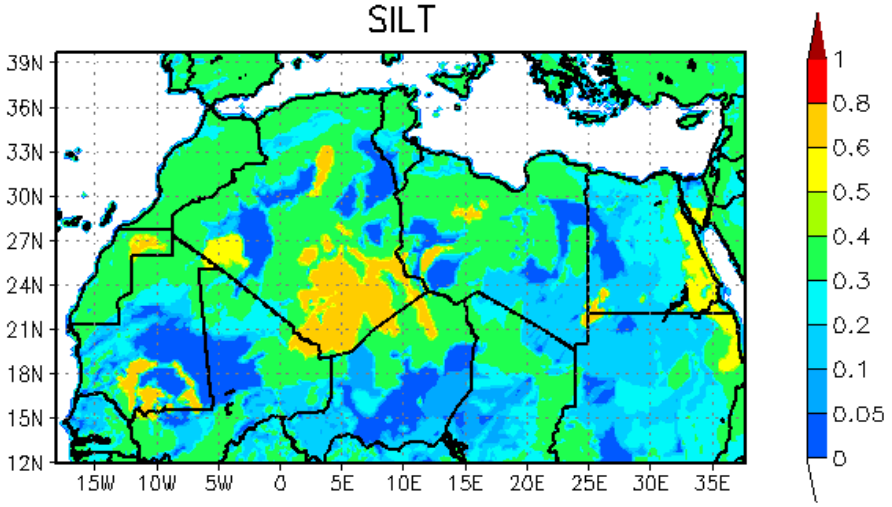

Figure 6: Silt fraction for North Africa

The twelve soil textures are mapped for North Africa domain.

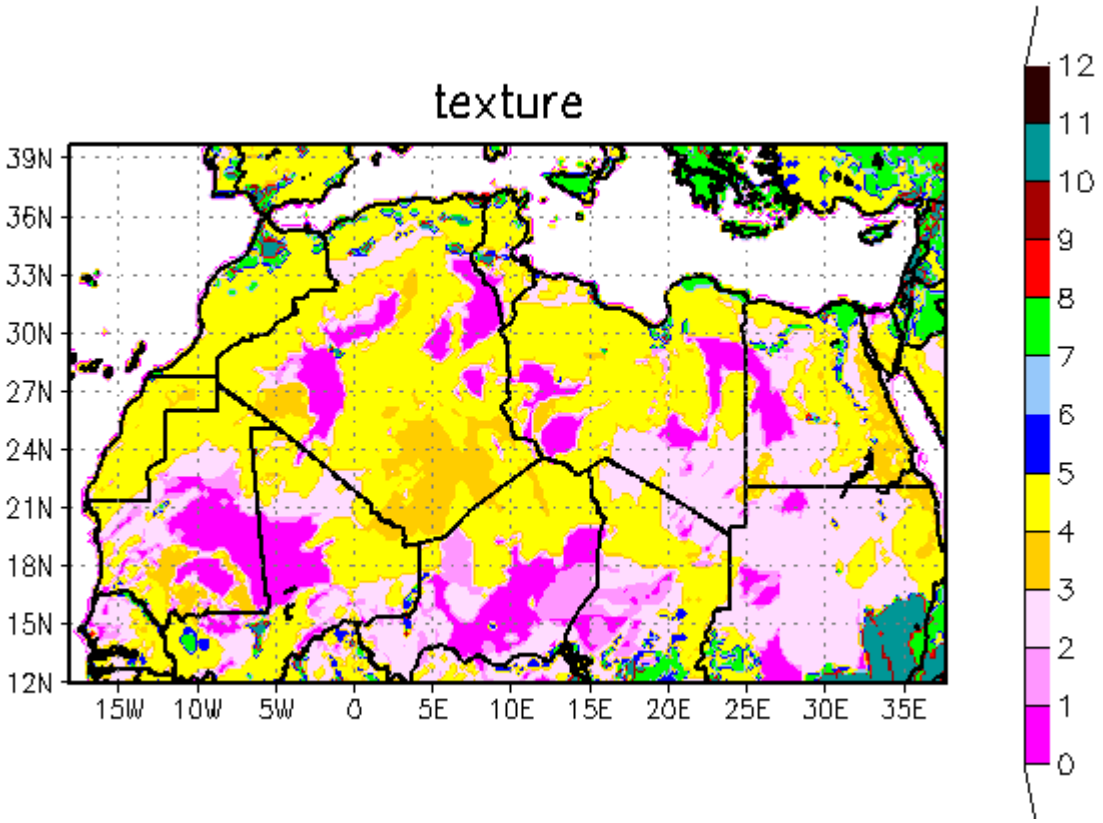

Figure7: soil textures map elaborate for SURFEX for North Africa

2.2.3 Soil aggregate distribution

Three-mode lognormal soil aggregate diameter distribution, *M(Dp)*, are associated to each texture class following *Zobler [1986]*: Table 2 reports the mass mean diameter *(M_{med}),* standard deviation *(σ),* and soil texture composition used to characterize each textural class *[Zakey et al., 2006]*.

$$\frac{dM(D_p)}{d\ln(D_p)} = \sum_{j=1}^{n} \frac{M_j}{\sqrt{2.\pi}.\ln(\sigma_j)}.\exp\frac{\left(\ln D_p - \ln D_{medj}\right)^2}{-2.\ln^2\sigma_j} \qquad (1)$$

Table 2: The 12 basic USDA soil texture indices and corresponding soil aggregate size distribution parameters.

	Mode 1			**Mode 2**			**Mode 3**		
soil type	*%*	D_{med}	σ	*%*	D_{med}	σ	*%*	D_{med}	σ
Sand	*90*	*1000*	*1.6*	*10*	*100*	*1.7*	*0*	*10*	*1.8*
Loamy sand	*60*	*690*	*1.6*	*30*	*100*	*1.7*	*10*	*10*	*1.8*
Sandy loam	*60*	*520*	*1.6*	*30*	*100*	*1.7*	*10*	*5*	*1.8*
Silt loam	*50*	*520*	*1.6*	*35*	*100*	*1.7*	*15*	*5*	*1.8*
Loam	*35*	*520*	*1.6*	*50*	*75*	*1.7*	*15*	*2.5*	*1.8*
Sandy clay loam	*30*	*210*	*1.7*	*50*	*75*	*1.7*	*20*	*2.5*	*1.8*
Silt clay loam	*30*	*210*	*1.7*	*50*	*50*	*1.7*	*20*	*2.5*	*1.8*
Clay loam	*20*	*125*	*1.7*	*50*	*50*	*1.7*	*30*	*1*	*1.8*
Sandy clay	*65*	*100*	*1.8*	*0*	*10*	*1.8*	*35*	*1*	*1.8*
Silty clay	*60*	*100*	*1.8*	*0*	*10*	*1.8*	*40*	*0.5*	*1.8*
Clay	*50*	*100*	*1.8*	*0*	*10*	*1.8*	*40*	*0.5*	*1.8*
Silt	*45*	*520*	*1.6*	*40*	*75*	*1.7*	*15*	*2.5*	*1.8*

Where j referring to the mode, M_j is the relative weight of each mode j, D_{medj} the geometric mean diameter and σ_j the standard deviation in µm.

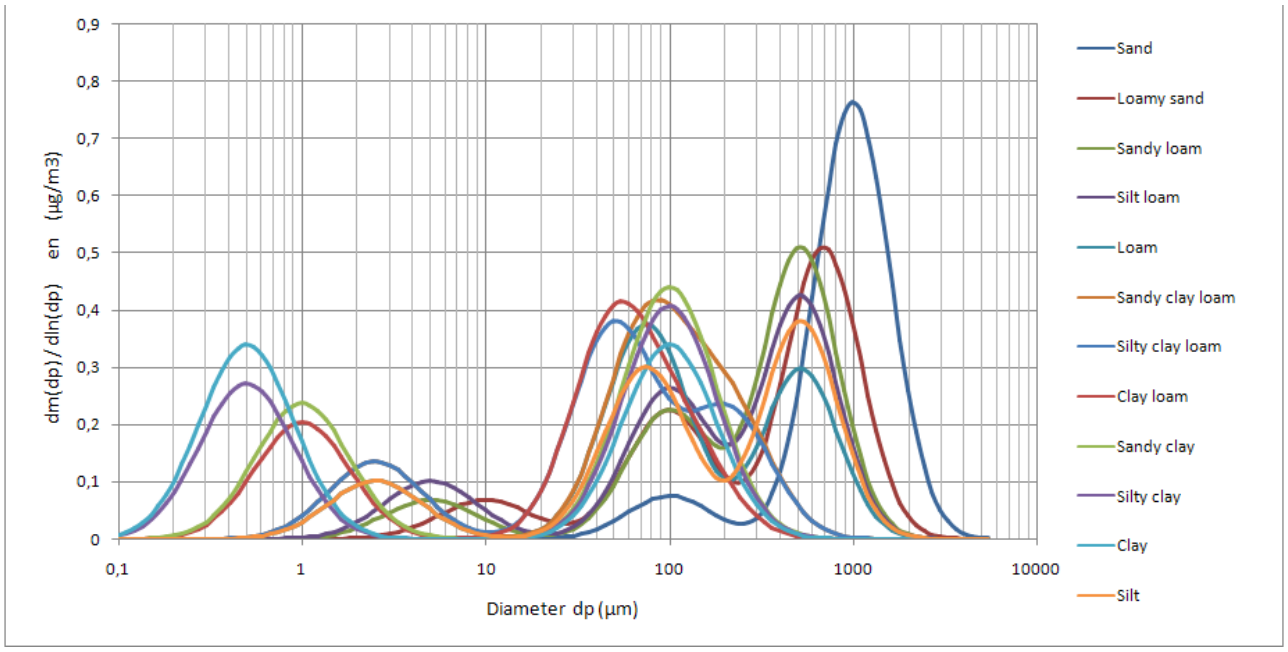

Figure 8: soil aggregate size distribution

Following *Marticorena [1995]*, the surface covered by each grain is assimilated to its basal surface. Thus a size distribution of the basal surface can be computed from the mass distribution, assuming spherical particles with the same density:

$$ds(D_p) = \frac{dM(D_p)}{\frac{2}{3} \cdot \rho_p \cdot D_p} \tag{2}$$

The total basal surface is

$$S_{total} = \int_{D_p} dS(D_p) dD_p \tag{3}$$

The normalized continuous relative distribution of basal surfaces:

$$dS_{rel} = \frac{ds(D_p)}{S_p} \tag{4}$$

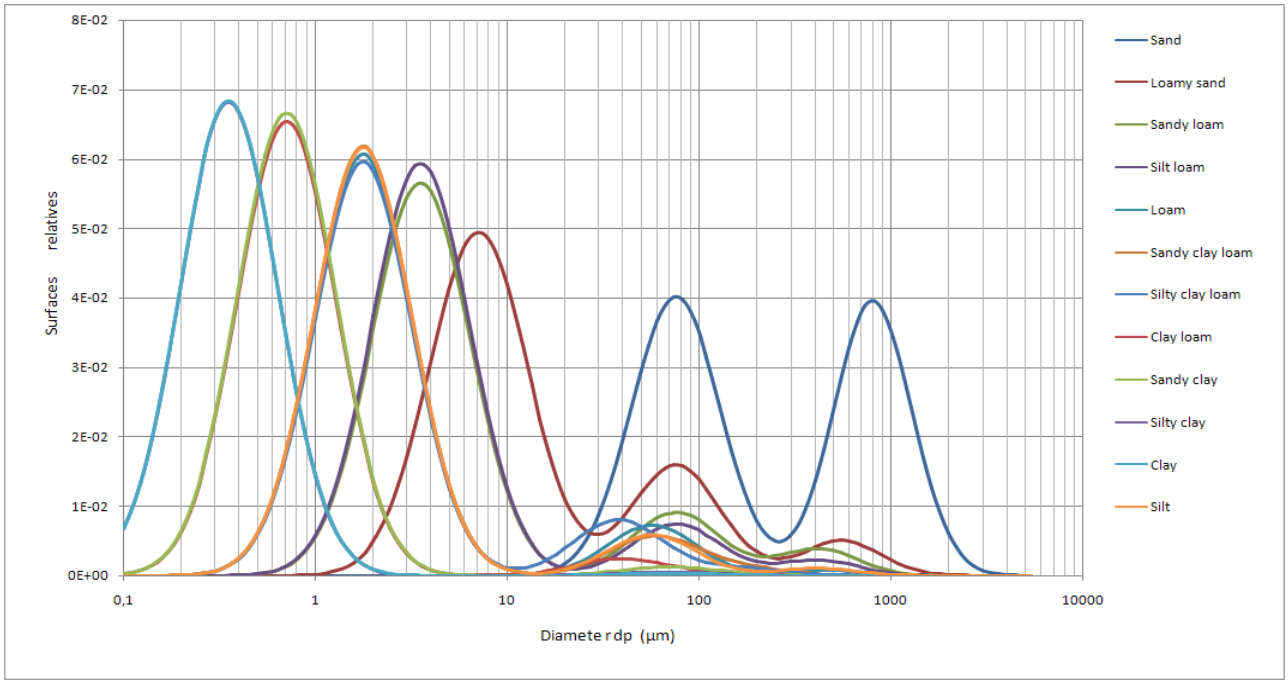

Figure 9: normalised relative distribution of basal surfaces

In our case, the potential of the fine particles in the soil is represented by the relative surface occupied by each particle. The figure 10 (a, b, c and d) illustrates the sum of relative surfaces of the particles divided into 4 populations: a) clay-size $D_p < 2\ \mu m$, b) small silt-size $2\mu m < D_p < 5\ \mu m$, c) large silt-size $5\ \mu m < D_p < 60\ \mu m$ and d) sand-size $D_p > 60\mu m$.

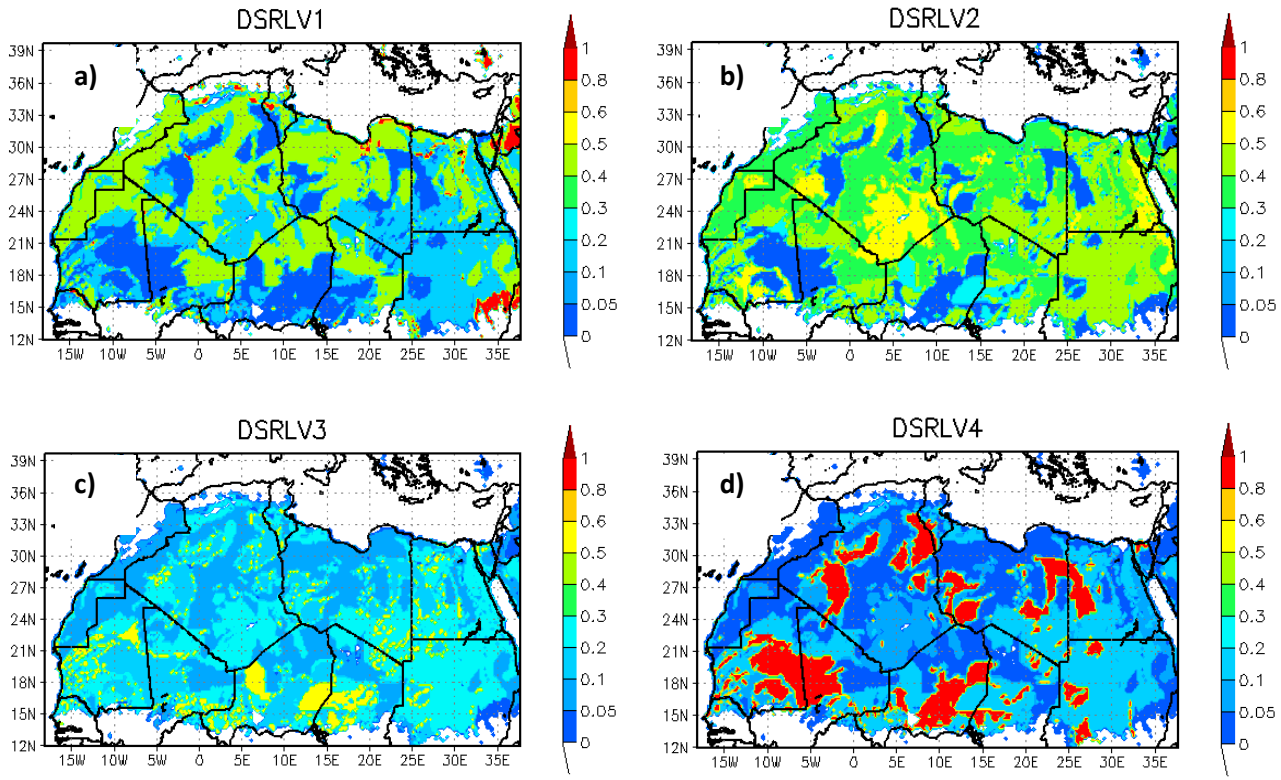

Figure 10: the sum of relative surface of soil particle with diameter comprise: a) Dp<2 µm, b)2µm <Dp<5µm, c) 5µm <Dp<60µm, and d) Dp>60µm

2.2.4 Thresholds friction velocity

The threshold friction velocity u_{*_t} is the minimal speed necessary to start the dust mobilization. It depends on the diameter of the particles, the surface roughness and the soil moisture *[Marticorena and Bergametti, 1995; Shao, 2001]*. Many formulations of the threshold friction velocity are proposed: *Bagnold [1941]*, *Iversen and White [1982]*, *Marticorena and Bergametti [1995]* and recently *Shao and Lu [2000]*. The semi-empirical expressions proposed by *Marticorena and Bergametti [1995]* are easier to use and provides a very satisfying estimation of the threshold friction velocity as a function of the particle diameter for terrestrial conditions.

For $0.03 < \mathrm{Re}_{*_t} < 10$

$$u_{*t}(D_p) = \frac{0.129 \quad K}{\left(1.928\ \mathrm{Re}_{*_t}^{0.092} - 1\right)^{0.5}} \tag{5}$$

For $\mathrm{Re}_{*_t} > 10$

$$u_{*_t}(D_p) = 0.12\,K\left[1 - 0.0858\ \exp\left(-0.0617\ \left(\mathrm{Re}_{*_t} - 10\right)\right)\right] \tag{6}$$

Where

$$a = 1331\ ;\ b = 0.38\ \ ;\ x = 1.56\ ;$$

$$K = \left(\frac{\rho_p g D_p}{\rho_a} \right)^{0.5} \left(1 + \frac{0.006}{\rho_p g D_p^{2.5}} \right)^{0.5}$$

et :

$$\mathrm{Re}_{*t} = aD_p^x + b \tag{7}$$

With $\rho_p = 2.65\ \mathrm{g/cm^3}$ the particle density, $\rho_a = 0.00123\ g/cm^3$ the air density and the factor 0.006 in both equations is $\mathrm{g.cm^{0.5}.s^{-2}}$.

According to *[Marticorena and Bergametti 1995],* this relation shows its limits for particles with a diameter less than 10 µm. To palliate to this problem concerning these particles, we assumed that their mobilization starts when the friction velocity exceeds 0.7 m/s. This value indicates the end of the rough regime and the beginning of the very rough regime in Dust REgional Atmospheric Modeling DREAM *[Nickovic et al., 2001]*. For the later, all types of the particles will be mobilized.

2.2.5 Drag partition

A drag partition affects the erosion threshold by two ways. On one hand, the roughness elements cover just a part of the surface and thus protect it from the aeolian erosion; on the other hand, they consume part of wind momentum that will not be available to initiate particle motion. This leads to a global decrease of wind shear stress acting on the erodible surface and then of the erosion efficiency *[Marticorena and Bergametti, 1995]*. A physical scheme of the drag partition between the roughness elements and the erodible surface was developed by *Marticorena and Bergametti [1995]*. The efficiency with which drag is partitioned between erodible and nonerodible soil is expressed as an increase f_{eff} in the threshold friction velocity u_{*_t} *[Marticorena and Bergametti, 1995]*.

$$f_{eff}(Z_0, z_{0s}) = 1 - \frac{\log\left(\frac{Z_0}{z_{0s}} \right)}{\log\left(0{,}35 \left(\frac{0.1}{z_{0s}} \right)^{0{,}8} \right)} \tag{8}$$

Where Z_0 is the roughness length for momentum and z_{0s} is the smooth roughness length.

Z_0 and z_{0s} are expressed in centimeter unit.

The roughness length of the erodible surface z_{0s} is estimated from the size of the erodible particles. Following *Greeley and Iversen [1985],* this roughness length is proportional to approximately 1/30 of the diameter of these particles.

$$z_{0s} = D_{med} / 30 \tag{9}$$

Where D_{med} is the median diameter of the coarsest population calculated for twelve considered textures.

The threshold friction velocity in a rough situation is:

$$u_{*t}\left(D_p, Z_0, z_{0s}\right) = \frac{u_{*t}\left(D_p\right)}{f_{eff}\left(Z_0, z_{0s}\right)} \tag{10}$$

2.2.6 Soil moisture effects

Soil water increases the threshold friction velocity u_{*t}, therefore reducing the amount of dust injected into the atmosphere. The water resists in the soil, this is due to the capillary forces on the surfaces of the soil and also to molecular adsorption. In SURFEX model, the soil moisture effects on u_{*t} are included, following the method of *Fecan et al., [1999]*. The maximum amount of the adsorbed water *w'* is an increasing function of the clay fraction in the soil. *Fecan et al., [1999]* proposed the calculation of *w'* as a function of clay content in the soil:

$$w' = 0{,}0014\left(\%\arg ile\right)^2 + 0{,}17\left(\%\arg ile\right) \tag{11}$$

The suggested equation expresses the increase in the threshold friction velocity in wet conditions u_{*t}^{w} by reference to the threshold friction velocity in dry conditions $u_{*t}d$:

$$\begin{cases} for\ \ w_g < w' : & \dfrac{u_{*t}^{w}}{u_{*t}^{d}} = 1 \\ for\ \ w_g > w' : & \dfrac{u_{*t}^{w}}{u_{*t}^{d}} = \left[1 + 1{,}21\left(w_g - w'\right)^{0{,}68}\right]^{1/2} \end{cases} \tag{12}$$

Here $w_g\,(kg.kg^{-1})$ is the gravimetric water content.

Since the ISBA scheme uses the volumetric soil water content $w_v\,(m^3 m^{-3})$, it is necessary to convert the ISBA volumetric water content to the gravimetric water content. At saturation, the volumetric water content $w_s\,(m^3.m^{-3})$ is given:

$$w_s = 0.489 - 0.126 M_{sand} \tag{13}$$

The bulk density of dry surface soil $\rho_{b,d}$ $kg.m^{-3}$ is:

$$\rho_{b,d} = \rho_p(1 - w_s) \qquad (14)$$

$$w_g = w_v \frac{\rho_l}{\rho_{b,d}} \qquad (15)$$

Where M_{sand} $kg.kg^{-1}$ is the mass fraction of sand in the soil, $\rho_p = 2650\,kg.m^{-3}$ is the mean soil particle density, and $\rho_l = 1000\,kg.m^{-3}$ is the liquid water density.

Figure 8 shows the *w'* for the North Africa domain.

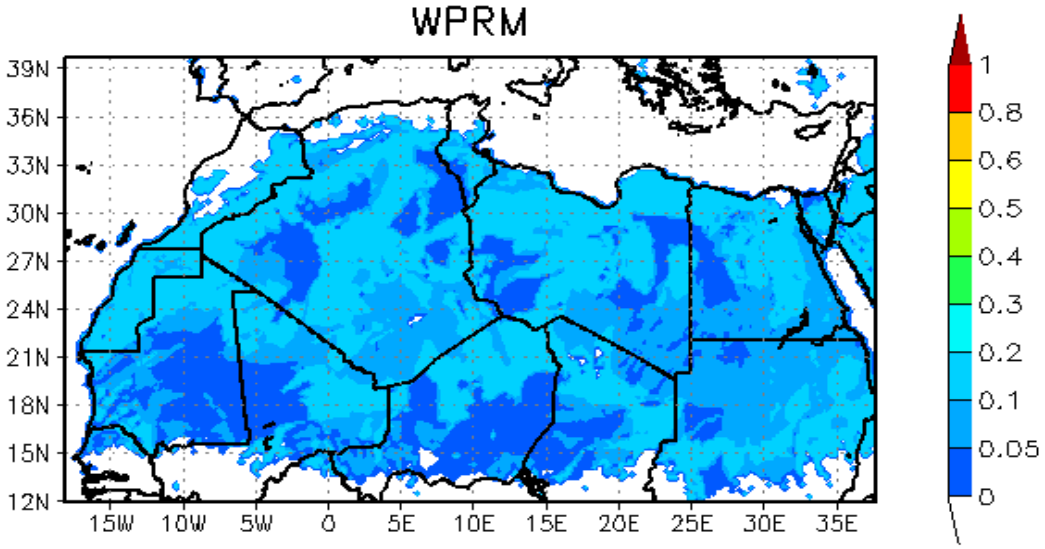

Figure 11: w' map on North Africa

Figure 12 shows the threshold friction velocity for North Africa

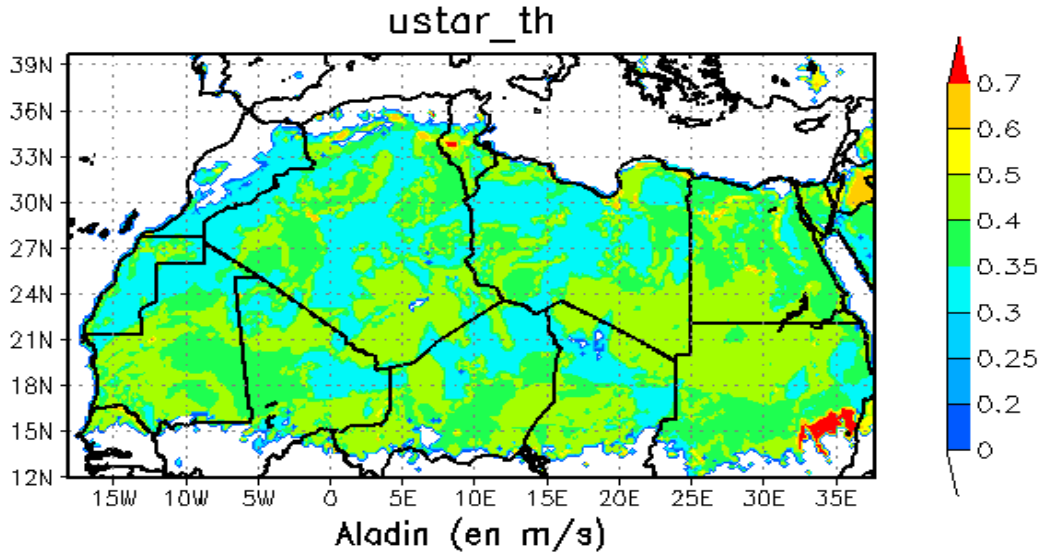

Figure 12: Threshold friction velocity on North Africa

2.2.7 Owen effect

The increase of the friction velocity due to the Owen effect is calculated as follow *[Zender et al. 2003]:*

$$u_{*_s} = u_* + 0.003\left(U_{10} - U_{10,t}\right)^2 \qquad (16)$$

Where U_{10} *et* $U_{10,t}$ are respectively the wind speed and the threshold wind speed at 10 m. The Owen effect is activated when the saltation processes starts.

2.2.8 Horizontal dust flux

The horizontal dust flux represents the mass of the particles passing the vertical surface area of infinity height and unit width per unit time. It substantially consists of particles moving in saltation. In order to take into account the soil aggregate distribution in the horizontal flux, the relation of *Marticorena and Bergametti [1995]* is used. This relation supposes that the contribution of each class of size on the total flux depends directly on the relative surface occupied by each class on the soil. The horizontal flux is then the sum of the relative contributions of the various classes of sizes in the domain of the considered particle.

$$G = a.E.c.\frac{\rho}{g}.u_*^3 \sum\nolimits_{D_p} \left(1 + \frac{u_{*_t}}{u_*}\right)\left(1 - \frac{u_{*_t}^2}{u_*^2}\right) dS_{rel}\left(D_p\right) dD_p \qquad (17)$$

Where E is the fraction of the erodible surface, $dS_{rel}(Dp)$ is the relative surface and $a=0.04$ is the global mass flux tuning factor determined at posterior through of the experimental model.

2.2.9 Vertical flux

The vertical flux represents the mass of the fine particles passing through an horizontal unit area per unit time. Many parameterization of the ratio of vertical to horizontal flux α were proposed. *Marticorena and Bergametti [1995]* proposes a relation according to the quantity of the fine particles available in the soil. They thus calculated this ratio according to the clay content for the soils having less than 20% clay. *Shao and al., [1993]* proposes a semi-empirical relation according to the potential energies necessary for the rupture of the cohesion forces; which maintain the fine particles and their setting in suspension. These energies are represented by the thresholds of erosion. In this notice the parameterization of Shao is used.

$$\alpha = \frac{F}{G} = \frac{2}{3} \times \frac{\rho_p}{\rho} \times \frac{\beta\gamma g}{\left[U_{*_t}(D_d)\right]^2} \qquad (19)$$

$\gamma = 2.5$ et

$$\beta = \left[0.125\times10^{-4}\ln(D_s)+0.328\times10^{-4}\right]\exp\left(-140.7.D_d+0.37\right) \qquad (20)$$

Where D_d et D_s in mm et β >0.

D_s : average diameter of the particles in saltation (~75µm) D_d *:* average diameter of the suspended particles (~6.7µm).

Then the sandblasting mass efficiency α is illustrates in figure 13.

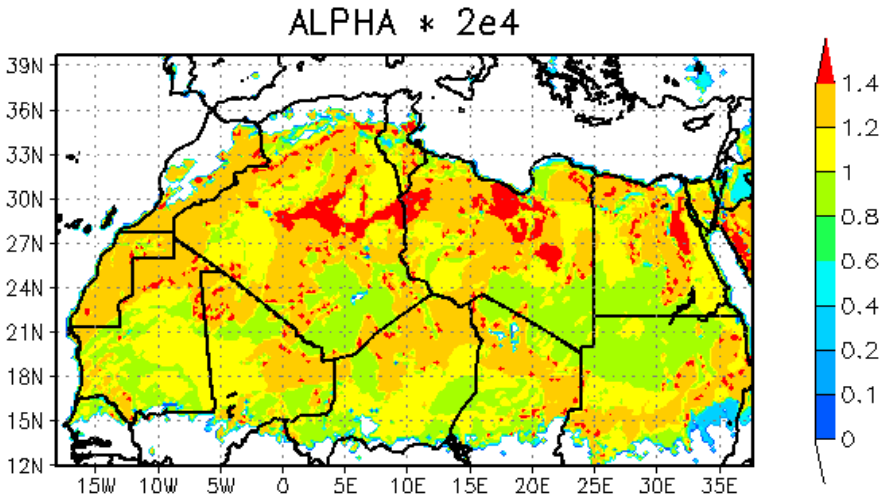

Figure 13: The sandblasting mass efficiency $\alpha\times2.10^4$ *for North Africa obtained by Shao 2003*

The vertical dust flux is fractioned in 3 modes following the AMMA parameterization.

	Mode 1	Mode 2	Mode 3
Mass fraction M_i	0.0008	0.0092	0.99
D_i *(µm)*	0.078	0.641	5.00
σ_i	1.75	1.76	1.70

2.2.10 Dry deposition

Dry deposition and sedimentation of aerosols are driven by the Brownian diffusivity

$$D_p = \left(\frac{kT}{6\pi\nu\rho_{air}.r_p}\right)C_c \qquad (21)$$

and by the gravitational velocity

$$V_{g.p} = \left(\frac{2g}{9\nu}\left(\frac{\rho_p}{\rho_{air}}\right)r_p^2\right)C_c \qquad (22)$$

where k is the Boltzmann constant, T the ambient temperature, ν the air kinematic velocity, ρ_{air} the air density, g the gravitational acceleration, ρ_p the aerosol density and

$C_c = 1 + 1.246 \frac{\lambda_{air}}{r_p}$ the gliding coefficient and λ_{air} is the mean free path of air molecules.

For details of the formulation refer to *Tulet et al. [2005]*.

2.3 Transport, gravitational settling and wet removal of dust aerosols

In order to treat the dynamic and physic processes relating to dust aerosol in atmospheric model, we introduced 9 additional advectable variable of type GFL (Grid-point field) in ALADIN code. These variables are related to the three modes for the dust aerosol in its three states: dry aerosol, aerosol in rain and aerosol in cloud. Horizontal advection, vertical advection and lateral diffusion of the GFL variable are previously coded in ALADIN. For the vertical diffusion, the scheme used for temperature and moisture is applied for aerosol diffusion. Thus the same exchange coefficient is used. For the sedimentation, the parameterization used in ORILAM scheme *[Tulet et al. 2005]* is adopted. The wet removal dust aerosol is calculated in ALADIN model using the SCAVenging submodel *[Tost et al. 2006]* developed for MesoNH. Four physical processes (Figure 14) relating to the wet deposition are treated by this scheme:

- Impaction scavenging by cloud droplets, the main process is the Brownian motion of dry aerosols and cloud droplets *[Pruppacher and Klett, 2000]* and impaction scavenging by raindrops depends mainly on Brownian motion, interception, and inertial impaction *[Slinn 1979]*.
- The in-cloud mass aerosol transfers into rain droplets by autoconversion and accretion processes.
- The aerosol mass sedimentation included in raindrops.
- The evaporation of rain releases the aerosols in atmosphere.

For details of formulation, refer to *[Tulet et al. 2010]*, *[Tost et al. 2006],* and *[Berthet, et al. 2010]*.

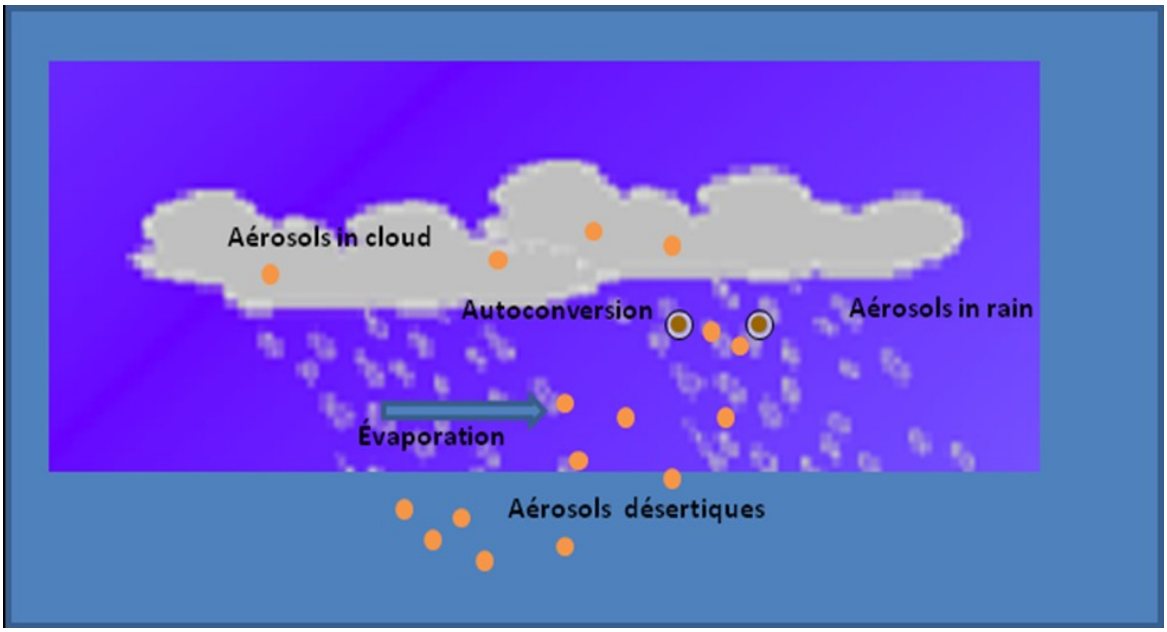

Figure 14: physical processes relating to the wet deposition treated in Aladin

3. The 2006 March 7-13West Africa dust storm simulation

The model version used in this study has an horizontal resolution of 24 km centred on North Africa, and 60 vertical levels. ALADIN is forced by the global model ARPEGE which provides lateral boundary conditions. In order to minimise the spinning up and establish reliable dust concentration conditions, we start the simulation from March 1st 2006 with 48 hour forecasts and the simulated dust concentration of the previous forecast was used as an update for the next-forecast model run.

3.1 Synoptic situation

The 2006, March 7-13 West African event simulated is characterized by an intense Harmattan wind at the surface. It was generated by a strong pressure gradient over West Africa between March 7th to 9th (Figure 15). The 850 hPa geopotential field from March, 8 at 12 UTC forecasted by ALADIN (Figure 16.a) shows a high pressure over Mauritania, whereas a deep low with a depression was located over Libya. This strong geopotential gradient which led to an intense Harmattan surface flux over the northern Niger and Chad (15 m.s−1), the northern Mali (12 m.s−1) and Mauritania (12 m.s−1) (Figure 15.a). The Inter-Tropical Discontinuity (ITD), which delineates the dynamic boundary between the Harmattan flux and the monsoon, can be observed at the surface on Figure 15.a, along a line extending from the north of Ivory Coast to the center of Nigeria. On March 10, 2006 (Figure 16.b), the high geopotential field centred over Mauritania decreased. As a consequence, the surface wind decreased over the Sahel region. The strong surface winds over the Sahel during the 7-13 March period leds to a strong dust storm which was readily observed from the MSG-SEVIRI satellite images *[Schmetz et al., 2006; Slingo et al., 2006]* (Figures 17). On

March 8, at 12 UTC (Figure 17.left), a high dust plume is observed spreading from the desert regions of Mali, Niger and Chad to the southwest part of the domain. The high dust concentration in the Sahelien African Layer (SAL) contrasts with the southerly cloudy monsoon air mass (in red). Over vegetation, the MSG-SEVIRI images cannot retrieve the dust signal which explains the strong limit observed between the dusty SAL and the more southern zone close to the Guinea Gulf (in blue). On March 12, at 12 UTC, the dust emission decreased in the desert region (white color in Figure 17.right), and the dust particles were then blown over the Guinea sea and north of Nigeria.

3.2 AOD during March 1st to 15th , 2006

The evolution of the AOD for Sahelian dust simulated by ALADIN is shown in the left part of Figure 18. A strong belt of high AOD appears from Chad to Senegal (Figure 18.a). Different AOD maxima have been simulated in the Chad (2.6), the southern part of Niger and the northern Nigeria (3.4) and Senegal (3). On March 10 (Figure 18.c), the plume of dust AOD spread to the South, reaching the Gulf of Guinea. In particular, three intense AOD maxima exceeding 3 have been simulated around Nigeria (from Benin to southern Chad and Cameroon). On March, 12, the intense dust plume continued its extension to the south over the Guinea Sea and the Atlantic Ocean but decreased on the whole domain (Figure 18.e). The evolution of the AOD has been observed by AQUA-MODIS satellite (right part of Figure 18). These data have been obtained from MODIS data collection 5 using MODIS on line visualization and Analysis System (MOVAS) developed at NASA (http://daac.gsfc.nasa.gov/techlab/giovanni/G3 manual Chapter 8 MOVAS.shtml). It is interesting to note the quite good agreement between the ALADIN simulation and the satellite observations during the event. Particularly it can be observed on March, 8, (Figure 18.b) that the dust plumes does not reach the Guinea Gulf and is still located in the north of Benin and centre of Nigeria. Except over southeast Nigeria and northern Cameroon, the location and intensity of high AOD, are comparable to the ones of MODIS and ALADIN. On March, 10, it is interesting to make relevant that the AQUA-MODIS satellite also retrieved three AOD maxima exceeding 3 in the same location around Nigeria (Figure 18.d). Moreover, the dust plume observed over Guinea and over the Atlantic Ocean, was reproduced in the simulation. On March, 12, the AQUA-MODIS observes some high AOD over Benin, Nigeria and Cameroon exceeding 3 in the coastal areas.

The simulated AOD are compared to AERONET photometers measurements located at Banizoumbou (Niger), DMN_Maine_Soroa (Niger), Capo_Verde, Cairo_EMA (Egypt), IER_Cinzana (Mali), Djougou (Benin), Ilorin (Nigeria), M'bour (Senegal), and Tamanrasset (Algeria). The results are illustrated in figure 19. Before the dust storm event of March 1st, 8th the AOD simulated are in well agreement, compared with those observed for the considered 9 stations.

The increase of the AOD observed on March 8th over the majority of the stations announces the beginning of the dust storm event. This increase is well envisaged by the ALADIN model. The Banizoumbou station is located in the Sahelian area of Niger. The strong winds observed in this area, generated a significant dust emission. AOD greater than 3 have been observed on March 7th and they reached values up to 4.0 on March 8th . At Banizoumbou, which is close to AERONET station (dust source zone), the simulated AOD estimates well the observed value but with one day of delay compared to the observed one. Over DMN_Maine_Soroa station the AOD simulated for the days March 8 to March 15 is in well agreement with the observed one, except for the peak observed for March 9th. This peak is due to local uprisings which is difficult to predict by numerical models. Cape-Verde is a station located in the Atlantic Ocean; it is affected by the dust aerosols transport. For this station, we notice that the AOD simulated during the dust storm event are in well agreement compared to the observed values except for March 9th when the AOD simulated are underestimated. The same remark can be made for Cairo_EMA station but for this station the AOD simulated for March 9th are over-estimated. Over IER_Cinzana station the AOD simulated for days March 8 to 11 are underestimated compared with the observed values. Then beyond March 11th, the simulated AOD are over-estimated. The AOD over the Ilorin station are underestimated; the maximum simulated AOD reached 3.1, whereas the photometers registered AODs above 4. At this stage, authors do not have concrete elements to understand if the origin of this underestimation is attributable to an underestimation of the simulated dust emission over Niger (surface winds) or to more local carbonaceous aerosols. Nevertheless, at Ilorin, the model was able to reproduce the delay in the increases of the AOD observed after March 9th. Thus, a systematic underestimation of AOD (about 1) also appeared at Djougou when the station was in the monsoon flux. This bias can be attributable to carbonaceous aerosols (black and organic carbon fractions) which are not included in the simulation. The AOD simulated over Mbour represents a peak at the endof-day on March 8th which exceeds 4 then to go down rapidly under 2 for the day afeter. Whereas, the values of AOD observed by this station are about 1.5 to 2.5 during the dust storm event to go down 1 from March 13th. The AOD simulated over Tamanrasset are in good agreement with those observed. Indeed, this station was not affected by this dust storm event.

3.3 Surface concentration during March 1st to 15th , 2006

Figure 20 shows the evolution of the surface concentration of dust aerosols compared to the observations from three stations: Banizoumbou, IER_Cinzana, and M'bour. The surface concentrations simulated over Banizoumbou at the beginning of the dust storm event (March 7th) are underestimated. Then the observed concentrations reached 2000 µg/m^3 on March 7th and 4000 µg/m^3 on March 8th while ALADIN predicted the concentration of 400 to 600 µg/m^3. The peak

observed on March 9th at this station is well simulated by the model. Beyond March 9th the model behaves very well compared to the observations. Over Cinzana, the evolution of the simulated concentrations during March 1st to march 9th are in oscillation with peaks exceeding the observed values during the periode extending from March 3 to march 7. During the dust storm event the concentration simulated are underestimated. Then observed concentrations attain 3400 μg/m^3 on March 8th and 3000 μg/m3 on March 10th . On the other hand, ALADIN predicted the values of 2400 μg/m3 for March 8th and 1000th μg/m3 for March 10th . Beyond March 11th, the model joined the observation. Over M'our, ALADIN reproduces with satisfaction the observed concentrations on March 9th where ALADIN predicts the concentration of 1000 μg/m3; while the observed ones are around 2000μg/m^3.

4. Conclusion

Through this work, we have contributed to the development of the ALADIN model by introducing atmospheric dust as a prognostic tracer in the model. The production and emission phases are simulated in ISBA scheme which is integrated in SURFEX. By the way, we introduced in the dust emission scheme: the geographic variation of the surface size dust distribution, size-dependent on energy thresholds for particle release during sandblasting, the *Marticorena* and *Bergametti (1995)* relationship in the horizontal saltation flux and the *Shao (2001)* formulate in the calculation of the sandbasting efficiency which is more compatible with SURFEX. The coupled system ALADIN_SURFEX is tested for March 7-13 West Africa dust storm. We validated our modelled dust plume against measurements available in the AMMA data base and the daily mean AOD from AQUA-MODIS satellite. The main results exposed in this notice are, in our point of view, interesting and viable. In extension, ALADIN has reproduced well the extension of the dust plumes. But in intensity, it has underestimated the AOD for the zones far from dust sources. The most plausible cause of that underestimation is the non conservative advection scheme used in the model. It is interesting to notice that the desert dust radiative effect is introduced in ALADIN model. For this purpose, a study of aerosols and weather forecast interaction is recommended.

Acknowledgments: I thank, Laurent Gomes, Claude Fischer, Pierre Tulet and Bachir Hamadache for their remarks and assistances. I also thank all those which contributed by far or for loan to the realization of this note.

References

Alfaro, S. C., and L. Gomes, Modeling mineral aerosol production by wind erosion: Emission intensities and aerosol distributions in source areas, *J. Geophys. Res*, 106, 18,075– 18,084, 2001

Andronache, C., T. Grönholm, L. Laakso, V. phillips, and A. Venäläinen, Scavenging of ultrafine particles by rainfall at a boreal site: observations and model estimations, *Atmos, Chem. Phys.*, 6, 4739-4754, 2006

Bagnold, R. A. , The Physics of Blown Sand and Desert Dunes, 265 pp., *Methuen*, *New York*, 1941

Brozková, R., M. Derková, M. Bellus, and A. Farda, Atmospheric forcing by ALADIN/MFSTEP and MFSTEP oriented tunings, *Ocean Sci*., 2, 113–121, 2006

Bubnová, R., G. Hello, P. Bénard, and J. F. Geleyn,: Integration of the fully elastic equations cast in the hydrostatic pressure terrainfollowing coordinate in the framework of the ALADIN NWP system, *Mon. Wea. Rev*., 123, 515–535, 1995

Buckley, R. L., Spatial Variation of Soil Type and Soil Moisture in the Regional Atmospheric Modeling System (U),*WSRC-TR* 2001-00119, March 2001

Callot, Y., B. Marticorena, and G. Bergametti, Geomorphologic approach for modelling the surface features of arid environments in a model of dust emission: application to the Sahara desert, *Geodinamica Acta* 13 245-270, 2000

Croft, B., U. Lohmann, R. V. Martin, P. Stier, S. Wurzler, J. Feichter, R. Posselt, and S. Ferrachat, Aerosol size-dependent below-cloud scavenging by rain and snow in the ECHAM5-HAM, *Atmos, Chem. Phys*., 9, 4653-4675, 2009

Cuesta, J., D. Edouart, M. Mimouni, P. H. Flamant, C. Loth, F. Gibert, F. Marnas, A. Bouklila, M. Kharef, B. Ouchène, M. Kadi, and C. Flamant, Multiplatform observations of the seasonal evolution of the Saharan atmospheric boundary layer in Tamanrasset, Algeria, in the framework of the African Monsoon Multidisciplinary Analysis field campaign conducted in 2006, *J. Geophys. Res*., Vol. 113, D00C07, doi:10.1029/2007JD009417, 2008

Fécan, F., B. Marticorena, and G. Bergametti, Parameterization of the increase of the aeolian erosion threshold wind friction velocity due to soil moisture for arid and semi-arid areas, *Ann. Geophysicae* 17, 149-157 1999

Foret, G., G. Bergametti, F. Dulac, and L. Menut, An optimized particle size bin scheme for modelling mineral dust aerosol, J. Geophys. Res., Vol. 111, D17310, doi:10.1029/2005JD006797,2006

Geleyn, J. F., Adaptation of spectral methods to non-uniform mapping (global and local), ECMWF Seminar Proceedings on "Recent developments in numerical methods for atmospheric modeling", 7–11 September 1998, 226–265, 1998

Greed, G., J. M. Haywood, S. Milton, A. Keil, S. Christopher, P. Gupta, E. J. Highwood, Aerosol optical depths over North Africa: Modeling and model validation, *J. Geophys. Res*., Vol. 113, D00C05, doi:10.1029/2007JD009457, 2008

Greeley, R., and J. D. Iversen , Wind as a Geological Process, *Cambridge Univ. Press*, New York. 1985

Grini, A., P. Tulet and L. Gomes, Dusty weather forecasts using the MesoNH mesoscale atmospheric model, *J. Geophys. Res.,* VOL. 111, D19205, doi:10.1029/2005JD007007, 2006

Henzing, J. S., D. J. L. Olivie, and P. F. J. Van Velthoven, A parameterization of size resolved below cloud scavenging of aerosols by rain, *Atmos, Chem. Phys*., 6, 3363-3375, 2006

Hoose, C., U. Lohmann, R. Bennartz, B. Croft, and G. Lesins, Global simulations of aerosol processing in clouds, *Atmos, Chem. Phys.*, 8, 6939-6963, 2008

Horányi, A., I. Ihàsz, and G. Radnoti, ARPEGE/ALADIN: A numerical weather prediction model for Central Europe with the participation of the Hungarian Meteorological Service, *idöjàràs*, 100, 277–301, 1996

Huth, R., R. Mlàdek, L. Metelka, P. Sedlàk, Z. Huthová , S. Kliegrová , J. Kysely, L. Pokorná, T. Halenka and M. Janousek, On the integrability of limited-area numerical weather prediction model ALADIN over extended time periods, *Stud. Geophys. Geod*., 47, 863−873. 2003

Iversen, J.D., B. R. White, Saltation threshold on Earth, Mars and Venus. *Sedimentology* 29, 111–119, 1982

Johnson, B. T., S. R. Osborne, J. M. Haywood, and M. A. J. Harrison, Aircraft measurements of biomass burning aerosol over West Africa during DABEX, *J. Geophys. Res*., Vol. 113, D00C06, doi:10.1029/2007JD009451, 2008

Johnson, B. T., B. Heese, S. A. McFarlane, P. Chazette, A. Jones, and N. Bellouin, Vertical distribution and relative effects of mineral dust and biomass burning aerosol over West Africa during DABEX, *J. Geophys. Res.,* Vol. 113, D00C12, doi:10.1029/2008JD009848, 2008

Laurent, B., B. Marticorena, G. Bergametti, J. F. Léon and N. M. Mahowald, Modeling mineral dust emission from the sahara desert using new surface properties and soil database, *J. Geophys. Res*., Vol. 113, D14218, doi:10.1029/2007JD009484, 2008

Mahowald, N., K. Kohfeld, M. Hansson, Y. Balkanski, S. P. Harrison, I. C. Printice, M. Schulz, and H. Rodhe, Dust sources and deposition during the last glacial maximum and current climate: A comparison of model results with paleodata from ice cores and marine sediments, *J. Geophys. Res*., 104, 15,895-15,916, 1999

Mahowald, N. M., A. R. Baker, G. Bergametti, N. Brooks, R. A. Duce, T. D. Jickells, N. Kubilay, J. M. Prospero, and I. Tegen, Atmospheric global dust cycle and iron inputs to the ocean, Global Biogeochem. Cycles, 19, GB4025, doi: 10.1029/2004GB002402, 2007

Marticorena, B., and G. Bergametti, Modeling the atmospheric dust cycle: 1. Design of a soil-derived dust emission scheme, J. Geophys. Res., 100, 16, 415-16, 430, 1995

Marticorena, B., and G. Bergametti, Two year simulations of seasonal and interannual changes of the Saharan dust emissions, Geophys. Res. Lett., 23, 1921-1924, 1996.

Marticorena, B., and G. Bergametti, B. Aumont, Y. Callot, C. N'Doume, and M. Legrand, Modeling the atmospheric dust cycle: 2. Simulation of the Saharan dust sources, J. Geophys. Res., 102, 4387-4404, 1997a

Marticorena, B., and G. Bergametti, D. A. Gillette, and J. Belnap, Factors controlling threshold friction velocity in semiarid and arid areas of the United States, *J. Geophys. Res*., 102, 23, 277-23, 287, 1997b

Marticorena, B., M. Kardous, G. Bergametti, Y. Callot, P. Chazette, H. Khatteli, S. Le Hégarat-Mascle, M. Maillé, J. L. Rajot, D. Vidal-Madjar, and M. Zribi, Surface and aerodynamic roughness in arid and semiarid areas and their relation to radar backscatter coefficient, *J. Geophys. Res.,* VOL. 111, F03017, doi:10.1029/2006JF000462, 2006

Martin, J. H., Glacial-interglacial CO_2 change: The iron hypothesis, *paleoceanography*, 5, 1-13, 1990

Masson, V. , A physically-based scheme for the urban energy balance in atmospheric models, *Boundary-Layer Meteorology*, 94, 357–397. 3.1, 2000

Masson, V., J. Champeaux, F. Chauvin, C. Meriguet, and R. Lacaze, A global database of land surface parameters at 1-km resolution in meteorological and climate models, *J. Clim*. , 16(9), 1261–1282. 3.2, 2003

Masuda, K., Y. Mano, H. Ishimoto, Aerosol Optical Thickness over the Oceans Derived from GMS-5 during Spring 2002 and 2003, *J. Meteor. Soc*. Japan, Vol. 83A, pp. 173-186, 2005

Menut, L., C. Schmechtig, and B. Marticorena, Sensitivity of the Sandblasting Flux Calculations to the Soil Size Distribution Accuracy, *American Meteor. Soc*., 2005

Menut, L., G. Forêt, and G. Bergametti, Sensitivity of dust concentrations to the model size distribution accuracy, *J. Geophys. Res*., Vol. 112, D10210, doi:10.1029/2006JD007766, 2007

Mlawer, E. J., S. J. Taubman, P. D. Brown, M. J. Iacono, and S.A. Clough, 1997: RRTM, a validated correlated-k model for the longwave. *J. Geophys. Res*., 102, 16,663-16,682

Morcrette, J., and Y. Fouquart, The overlapping of cloud layers in shortwave radiation parameterizations, *J. Atm. Sci*. , 43(4), 321–328. 3.1, 1986

Nicholson, S. E., C. J. Tucker, and M. B. Ba, Desertification, drought, and surface gegetation: An example from the West African Sahel, *Bull. Am. Meteorol. Soc*., 79, 815-829, 1998

Nickovic, S., and S. Dobricic, A model for long-rang transport of desert dust, *Mon Weather Rev*, 124, 2537-2544, 1996

Nickovic, S., G. Kallos, A. Papadopoulos, and O. Kakaliagou, Model for prediction of desert dust cycle in the atmosphere, *J. Geophys. Res*., Vol. 106, NO. D16, PAGES 18,113-18,129, AUGUST 27, 2001

Noilhan, J. And S. Planton: A simple parameterization of land surface processes for meteorological models. *Mon. Wea. Rev*. 117, 536-549, 1989

Noilhan, J., and M. J.F., The ISBA land surface parameterization scheme., *Global and Plan. Change*, 13, 145–159. 3.1, 1996

Osborne, S. R., B. T. Johnson, J. M. Haywood, A. J. Baran, M. A. J. Harrison and C. L. McConnell, Physical and optical properties of mineral dust aerosol during the Dust and Biomass-burning Experiment, *J. Geophys. Res*., Vol. 113, D00C03, doi:10.1029/2007JD009551, 2008

Perlwitz, J., I. Tegen, and R. L. Miller, Interactive soil dust aerosol model in the GISS GCM: 1. Sensitivity of the soil dust cycle to radiative properties of soil dust aerosols, *J. Geophys. Res*., 106, 18,167-18,192, 2001

Prospero, J. M., Long-term measurements of the transport of African mineral dust to the southeastern United States: Implications for regional air quality, *J. Geophys. Res*., 104, 15,917-15,928, 1999

Pruppacher, H., and J. Klett, Microphysics of Clouds and Precipitation. *Kluwer Academic Publishers*, 2000

Radnóti, G., Comments on "A spectral limited-area formulation with time-dependent boundary conditions applied to the shallowwater equations". *Mon. Wea. Rev*., 123, 3122–3123, 1995

Ratmeyer, V., W. Balzer, G. Bergametti , I. Chiapello, G. Fischer, U. Wyputta, Seasonal impact of mineral dust on deep-ocean particle flux in the eastern subtropical Atlantic Ocean, *Marine Geology* 159, 241-252, 1999

Shao, Y., M. R. Raupach, and P. A. Findlater, Effect of saltation bombardment on the entrainment of dust by wind, *J. Geophys. Res.*, 98, 12,719-12,726, 1993

Shao, Y., M. R. Raupach, and J. F. Leys, A model for predicting aeolian sand drift and dust entrainment on scales from paddock to region, Aust. J. Soil Res., 34, 309-342, 1996

Shao, Y., and M. Leslie, Wind erosion prediction over the Australian continent, *J. Geophys. Res.,* 102,30,091-30,105,1997

Shao, Y., and I. Lu, A simple expression for wind erosion threshold friction velocity, *J. Geophys. Res.*, *105*, 22,437–22,443, 2000

Shao, Y. , A model for mineral dust emission, J. Geophys. Res., 106, 20,239–20,254. 2001

Shao, Y., Y. Yang, J. Wang, Z. Song, L. M. Leslie, C. Dong, Z. Zhang, Z. Lin, Y. Kanai, S. Yabuki, and Y. Chun, Northeast Asian dust storms: Real-time numerical prediction and validation, J. Geophys. Res., 108(D22), 4691, doi:10.1029/2003JD003667, 2003

Slinn, W., Atmospheric sciences and power production. Precipitation Scavenging. *U. S. Department of Energy*, Washington, D.C. chap. 11., 1979

Swap, R., M. Garstang, S. Greco, R. Talbot, and P. Kallberg, Saharan dust in the Amazon Basin, *Tellus, Ser. B*, 44, 133-149, 1992

Tegen, I., and I. Fung, Modeling of mineral dust in the atmosphere: Sources, Transport, and optical thickness, *J. Geophys. Res.*, 99(D11),22,897-22,914, 1994

Tegen, I., A. A. Lacis, and I. Fung, The influence on climate forcing of mineral aerosols from disturbed soils, *Nature*, 380, 419-422, 1996

Tegen, I., B. Heinold, M. Todd, J. Helmert, R. Washington, and O. Dubovik, Modelling soil dust aerosol in the Bodélé depression during the BoDEx campaign, *Atmos, Chem. Phys*., 6, 4345-4359, 2006

Tost, H., P. Jöckel, A. Kerkweg, R. Sander, and J. Lelieveld, Technical note: A new comprehensive SCAVenging submodel for global atmospheric chemistry modelling. *Atmos. Chem. Phys*., 6, 565-574, 2006

Tulet, P., V. Crassier, F. Cousin, K. Suhre, and R. Rosset, ORILAM, a three-moment lognormal aerosol scheme for mesoscale atmospheric model: Online coupling into the Meso-NH-C model and validation on the Escompte campaign, *J. Geophys. Res*., VOL. 110, D18201, doi:10.1029/2004JD005716, 2005

Tulet, P., K. Crahan_Kaku, M. Leriche, B. Aouizerats, S. Crumeyrolle, Mixing of dust aerosols into a mesoscale convective system Generation, filtering and possible feedbacks on ice anvils, *Atmos. Res*. 96 (2010) 302-314

Váňa F., Physical parameterizations in the ALADIN model. *Meteorol. zpr*., **51**, 33-44 1998

Zakey, A. S., Imlementation and testing of a desert dust module in a regional climate model, *Atmos. Chem. Phys*., 6, 4687-4704, 2006

Zender, C. S., H. Bian, and D. Newman, Mineral Dust Entrainment and deposition (DEAD) model: Description and 1990s dust climatology, *J. Geophys. Res*., VOL. 108, NO. D14, 4416, doi:10.1029/2002JD002775, 2003

Zobler, L., A World soil file for global climate modelling, *Tech. Rep.* NASA-TM-87802, 32 pp., 1986

Results

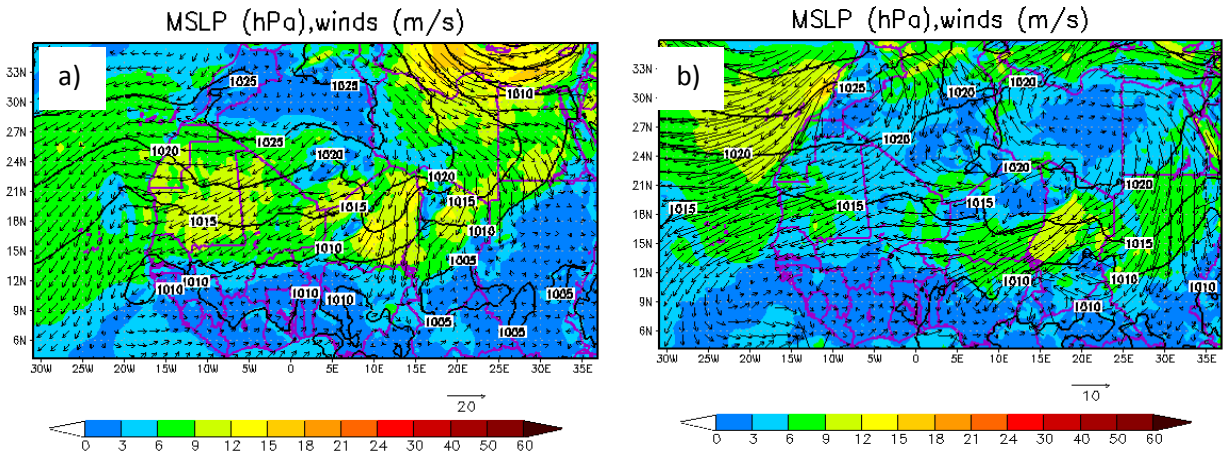

Figure 15: Mean sea level pressure (hpa) and wind speed at 10m on March 8th (a) and 10th (b) 2006

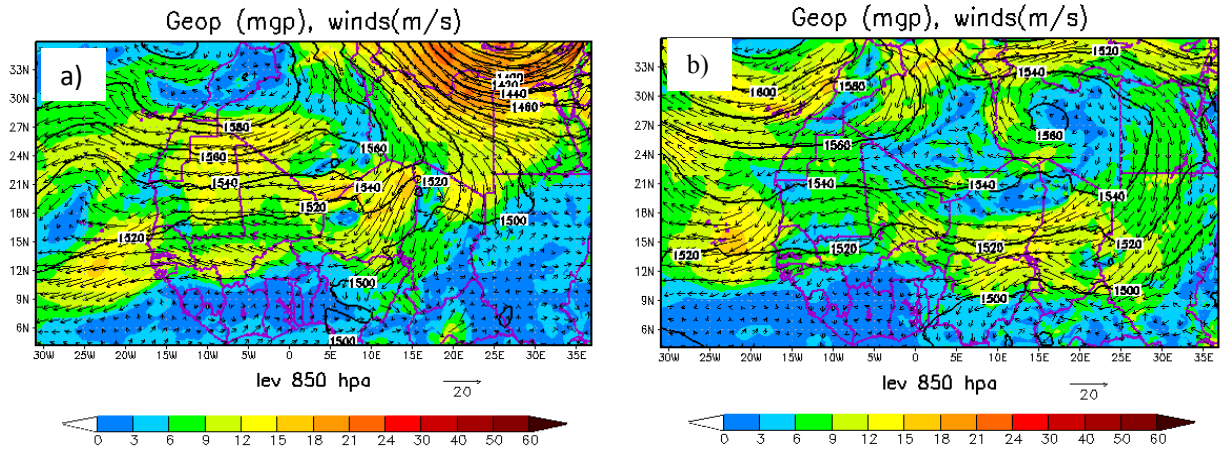

Figure 16 : The geopotential at 850 hPa (in meters) and wind speed on March 8th (a) and 10th (b) 2006

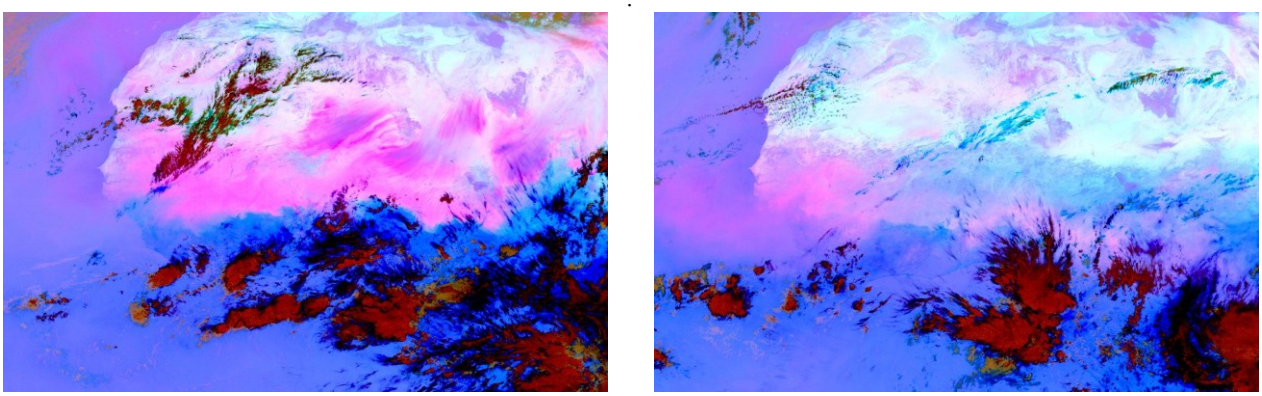

Figure 17: MSG-SEVIRI satellite images over West Africa for March 8, 2006 at 12 UTC (left) and March 12, 2006 at 12 UTC (right), pink color represent for dust, black for cirrus, red for high level cloud, brown for the mid-level cloud, and white for desert surface.

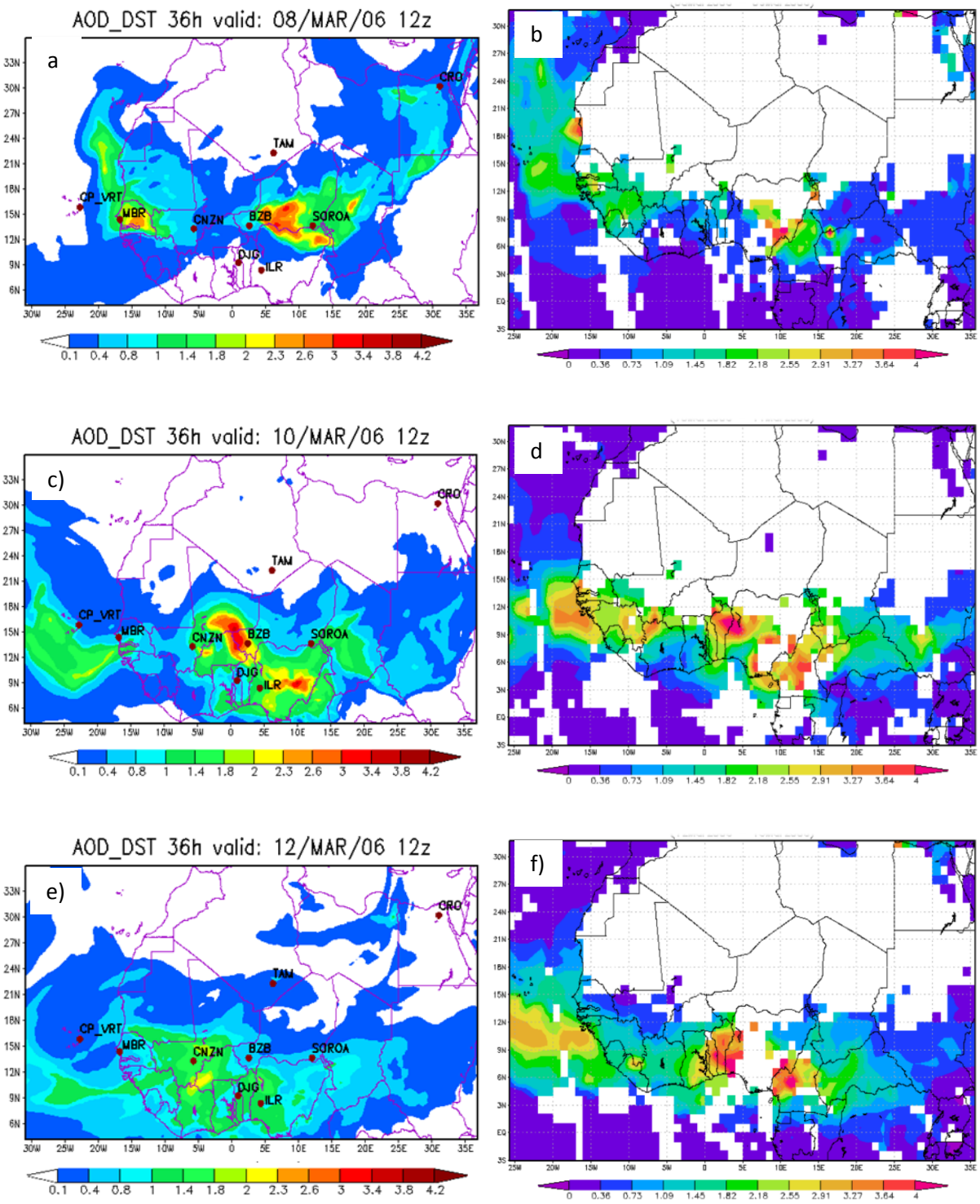

Figure 18: AOD simulated by ALADIN on March 8 at 12 UTC (a), March 10 at 12 UTC (c) and March 12 at 12 UTC (e), 2006. The daily mean AOD from MODIS/AQUA satellite images on March 8 (b), March 10 (d) and March 12 (f), 2006.

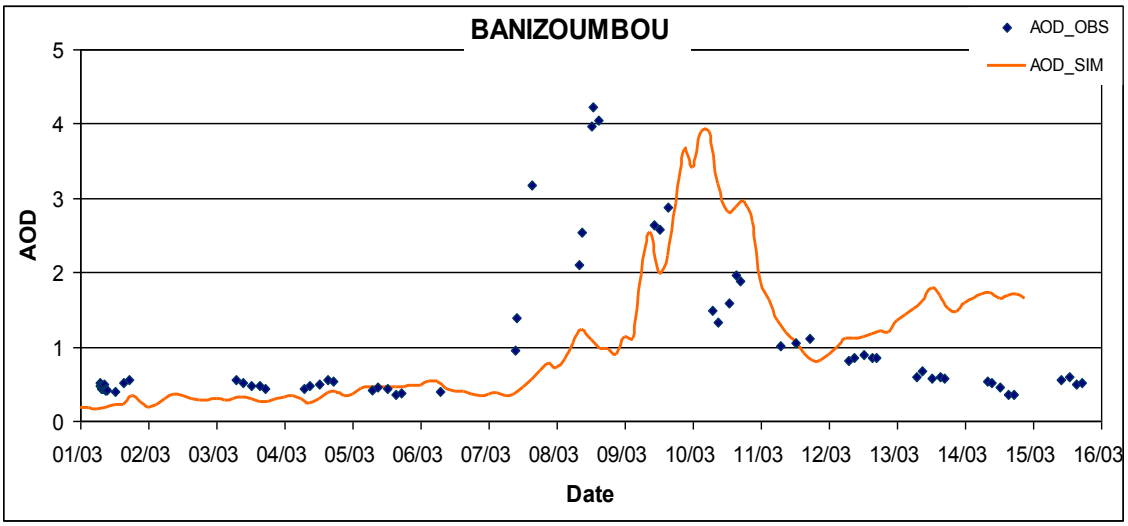
BANIZOUMBOU
AOD_OBS
AOD_SIM
AOD
5
4
3
2
1
0
01/03 02/03 03/03 04/03 05/03 06/03 07/03 08/03 09/03 10/03 11/03 12/03 13/03 14/03 15/03 16/03
Date

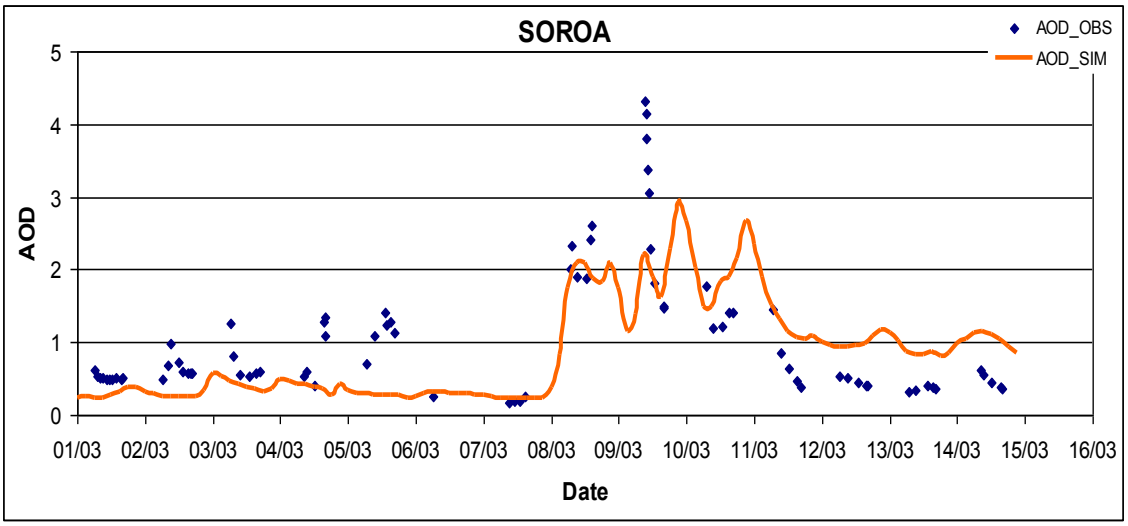
SOROA
AOD_OBS
AOD_SIM
AOD
5
4
3
2
1
0
01/03 02/03 03/03 04/03 05/03 06/03 07/03 08/03 09/03 10/03 11/03 12/03 13/03 14/03 15/03 16/03
Date

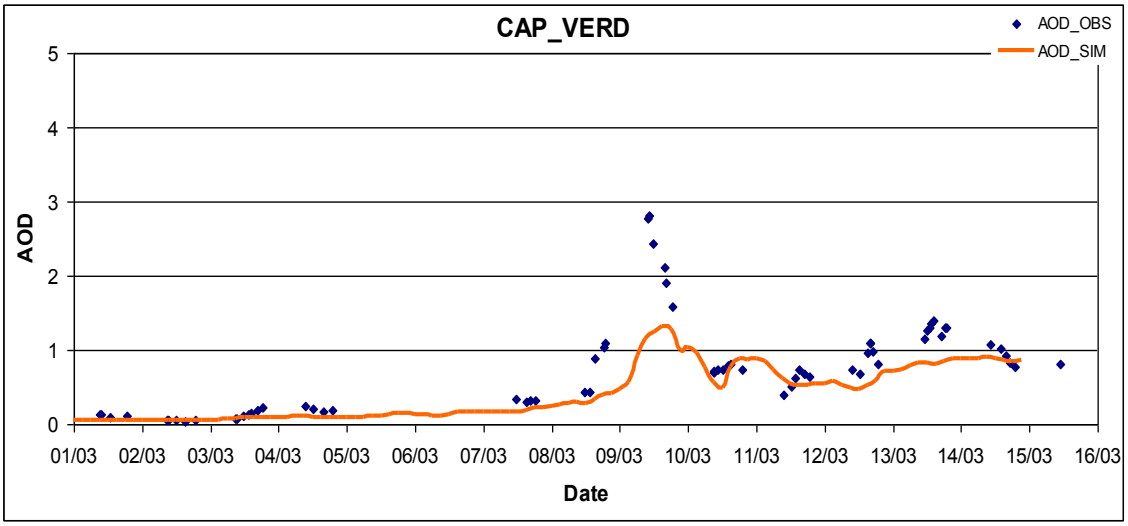
CAP_VERD
AOD_OBS
AOD_SIM
AOD
5
4
3
2
1
0
01/03 02/03 03/03 04/03 05/03 06/03 07/03 08/03 09/03 10/03 11/03 12/03 13/03 14/03 15/03 16/03
Date

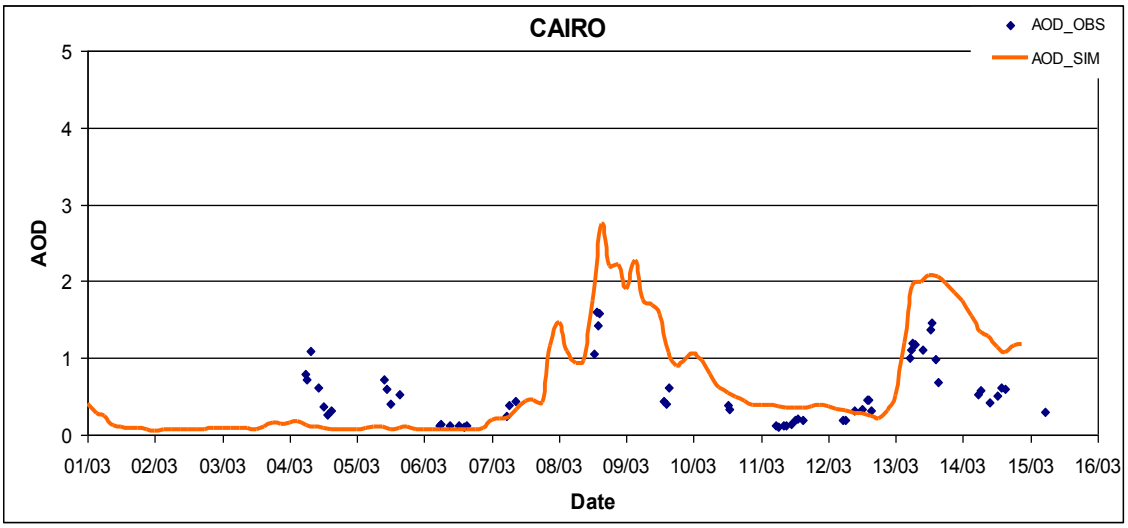
CAIRO
AOD_OBS
AOD_SIM
AOD
5
4
3
2
1
0
01/03
02/03
03/03
04/03
05/03
06/03
07/03
08/03
09/03
10/03
11/03
12/03
13/03
14/03
15/03
16/03
Date

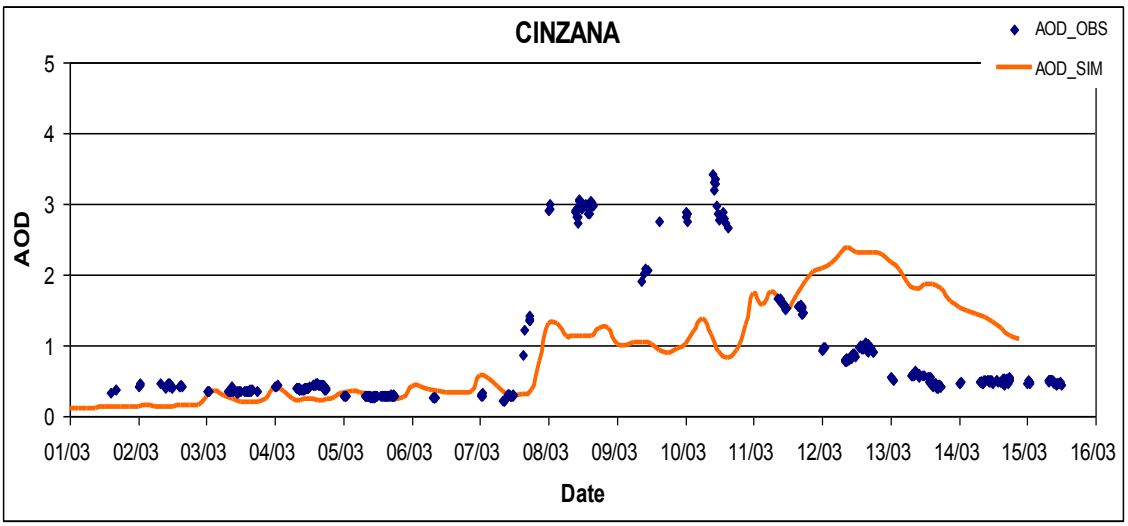
CINZANA
AOD_OBS
AOD_SIM
AOD
5
4
3
2
1
0
01/03
02/03
03/03
04/03
05/03
06/03
07/03
08/03
09/03
10/03
11/03
12/03
13/03
14/03
15/03
16/03
Date

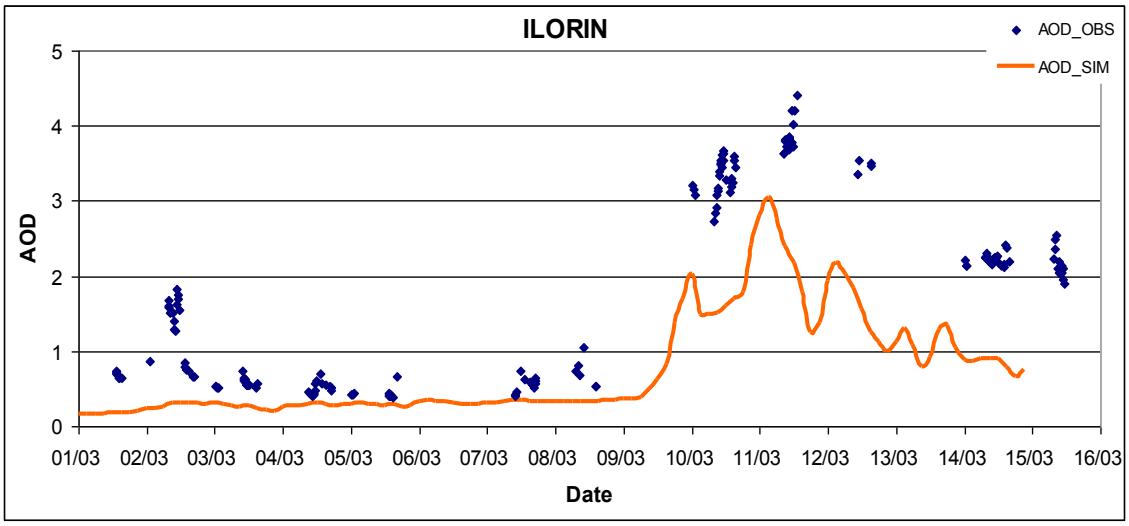
ILORIN
AOD_OBS
AOD_SIM
AOD
5
4
3
2
1
0
01/03
02/03
03/03
04/03
05/03
06/03
07/03
08/03
09/03
10/03
11/03
12/03
13/03
14/03
15/03
16/03
Date

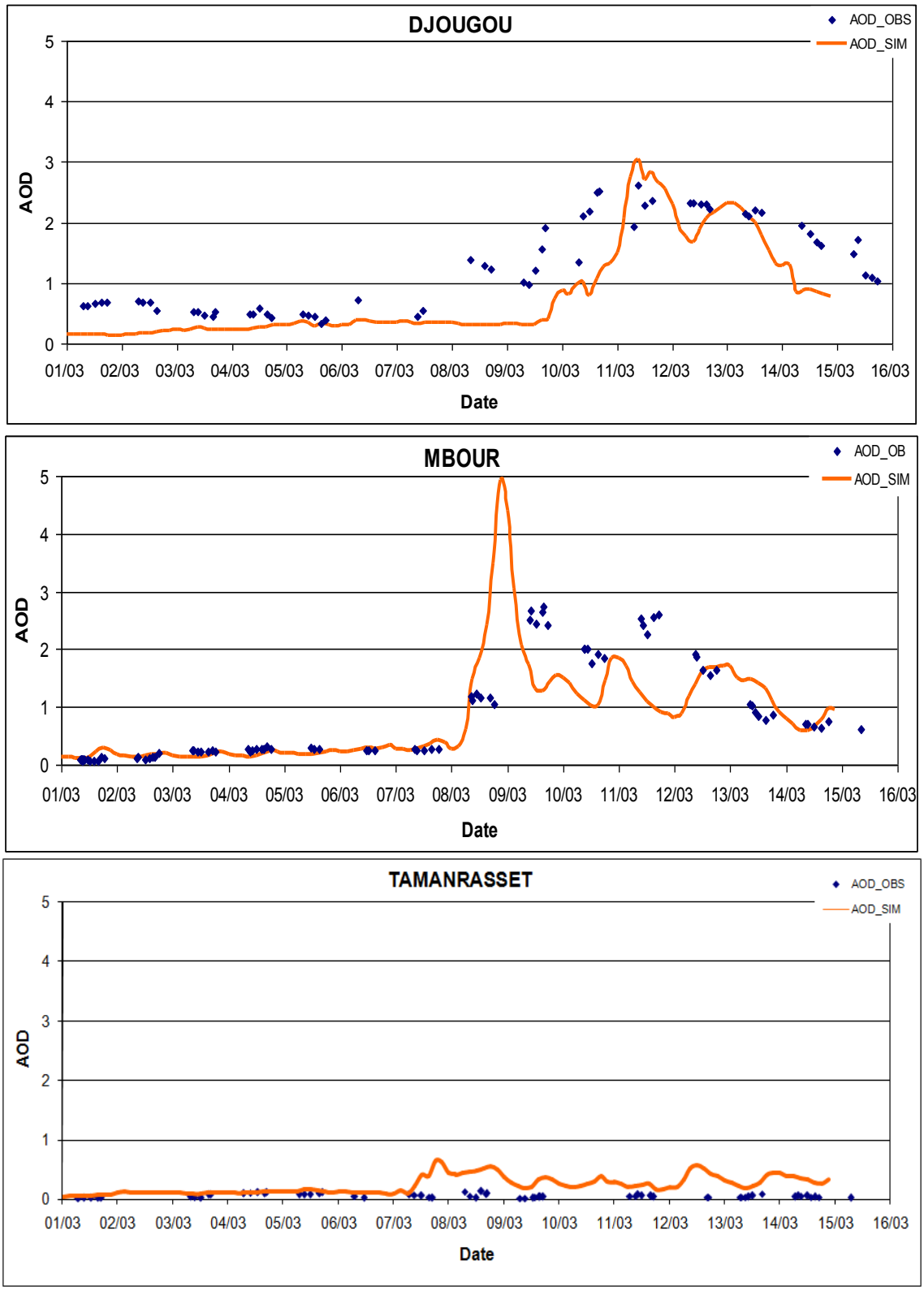

Figure 19 : The Evolution of the AOD simulated by ALADIN between 2006 March 1 and 15, 2006, at Banizoumbou, DMN_Maine_Soroa , Capo Verde, Cairo_EMA, IER_Cinzana, Ilorin, Djougou, M'bour and Tamanrasset. *The Dots represent the photometer observed values.*

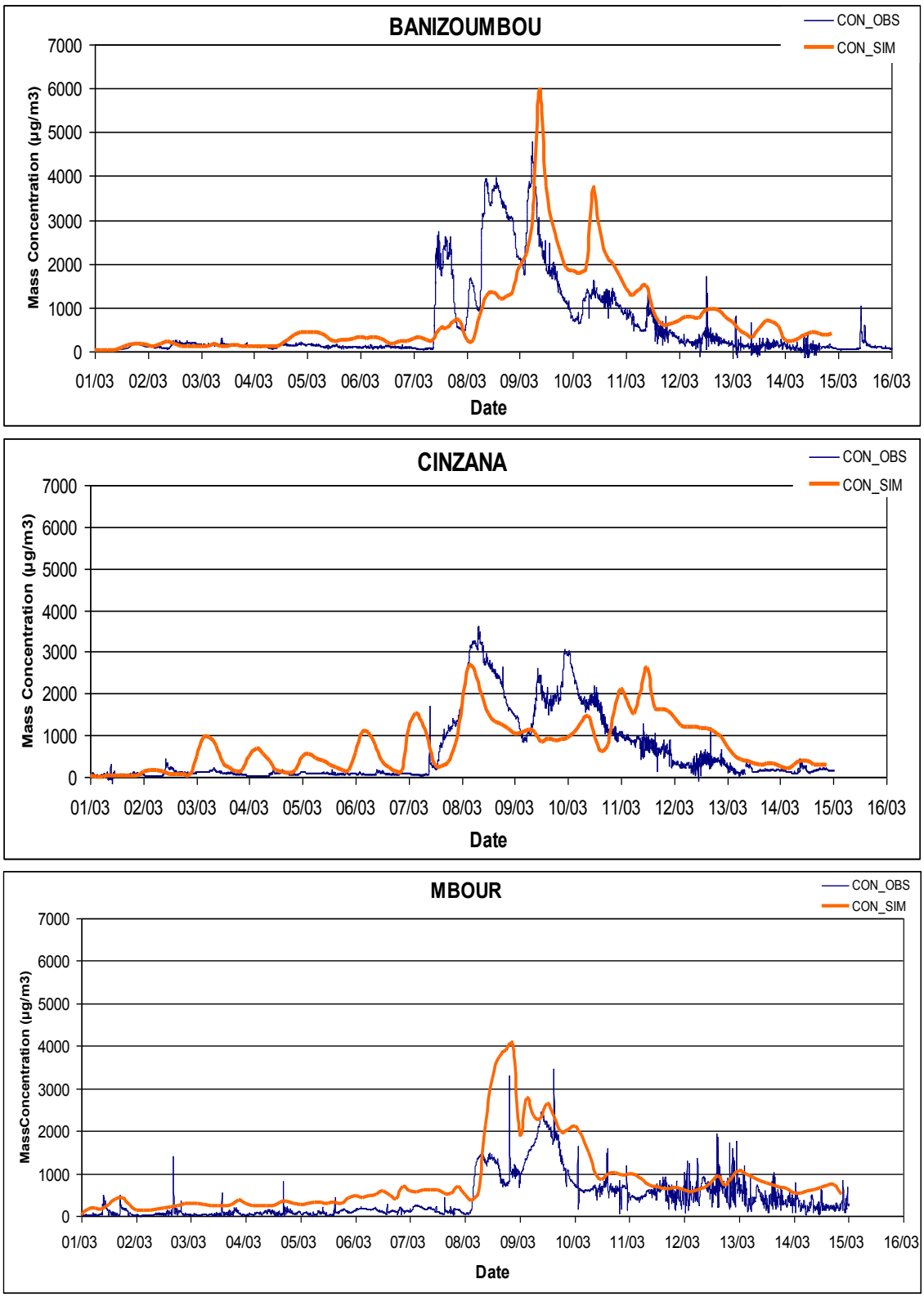

Figure 20 : The Evolution of the dust surface concentration simulated by ALADIN between 2006 March 1 and 15, 2006, at Banizoumbou, IER_Cinzana, and M'bour (red line) and surface dust concentration observed values (blue line).